THE STRUCTURE OF CLUSTERS OF GALAXIES AND THE ANGULAR SIZE-REDSHIFT TEST

Thesis by

Paul Hickson

In Partial Fulfillment of the Requirements

for the Degree of

Doctor of Philosophy

California Institute of Technology

Pasadena, California

1976

(Submitted March 16, 1976)

ACKNOWLEDGMENTS

I owe a great deal to many people for friendship, advice, and intellectual stimulation during the course of this work, and my graduate career. It is not possible to name everyone, so I offer my apologies and thanks to anyone I may have missed.

My wife Cathie, in addition to providing constant companionship and emotional support, spent innumerable hours helping with all phases of the work leading to this thesis. From squinting at faint stars on cold nights and small specks on dark plates to the preparation of the manuscript, her help was invaluable.

I am in debt to Jim Gunn, my thesis advisor, for providing suggestions, advice and encouragement, while allowing me freedom to follow my interests. He has provided unhesitating help both in this research, and other academic ventures, as well as assistance in administrative and financial matters.

I am grateful to all members of the faculty for the role they have played in my education and the example they have set by their own work.

I have benefited greatly from interaction with many others, particularly John Kormendy, Doug Richstone, Ed Turner, Richard Green, Barry Turnrose, Gus Oemler,

Paul Schechter, Steve Shectman, Trinh Thuan, John Hoessel, Jorge Melnick, Doug Rabin and Scott Tremaine to name a few.

I would like to thank Ranny Adams for skillful assistance at the telescope and conversation on cloudy nights.

I am particularly grateful to Helen Holloway, for help, advice, conversation, and for typing all of the tables in this thesis.

I am grateful to the National Research Council of Canada and the California Institute of Technology for financial support.

I would particularly like to thank Drs. Gunn and Oke for providing data in advance of publication.

ABSTRACT

An angular size-redshift cosmological test is presented based on the projected separations between bright cluster galaxies as the size statistic. The method is applied to 95 clusters of galaxies with redshifts ranging from .02 to .46 yielding a value of the deceleration parameter before evolution of $q_o = -.9$. After correcting for known evolutionary effects we obtain $q_o = -.8$. The formal standard deviation in q_o at these values is .2, which corresponds to an uncertainty of about .4 at $q_o = 0$. It is argued that the selection criteria for the sample, and the observed behavior of the cluster size dispersion with redshift precludes the existence of any major selection or evolutionary effects in the data.

Structure parameters are presented for a sample of 64 cosmologically near clusters, and correlated with Rood and Sastry type. New type classifications are presented for 23 clusters. Mean surface density profiles are determined for the various cluster types. It is found that many clusters are deficient in separations of one to two Mpc.

TABLE OF CONTENTS

INTRODUCTION

This thesis is divided into two parts, each in the form of a paper submitted to the Astronomical Journal, and intended to be independently readable. Some redundancy is unavoidable with this approach but it is hoped that this will not detract from the organization of the thesis. The two parts should be read sequentially as the first provides a foundation for the second. Part I deals with the problem of finding a cosmologically useful "standard meterstick" based on the sizes of clusters of galaxies, and cluster properties that may affect such a parameter are considered. Part II develops an angular size-redshift test based on the size parameter of Part I. The test is applied in Part II to a relatively large number of clusters of galaxies to yield a value of the deceleration parameter q_o.

PART I

THE STRUCTURE OF NEARBY CLUSTERS OF GALAXIES

I. INTRODUCTION

Clusters of galaxies are perhaps the largest well defined entities in the universe, which makes them powerful tools for probing its structure. Probably the simplest observational data that can be obtained from a cluster are the positions of its brightest galaxies. Positions are easy to measure, even for the most distant clusters, as one merely requires that the galaxies be visible on deep photographic plates. "Sizes" of clusters deduced from such measurements provide a direct cosmological test via the angular size-redshift diagram (Zwicky, 1957, Sandage, 1961). This test, while free from many of the systematic errors and uncertainties of the better known magnitude-redshift test (Sandage and Hardy, 1973, Gunn and Oke, 1975) and the galaxy angular diameter-redshift test (Sandage, 1961) has not gained popularity for several reasons. The sizes of clusters as conventionally measured display a considerable scatter due to the variety of cluster types. One is forced to select only rich, relaxed clusters whose shape is relatively well defined in order to reduce the dispersions. Zwicky (1957) has suggested that these clusters are well represented by an isothermal distribution, and introduced the "core radius" as a size parameter. Recent measurements have been made by Bahcall (1975) and Austin and Peach (1974).

Unfortunately the core radius ir rather sensitive to the assumed location of the center of the cluster, and to any departures from spherical symmetry. A second parameter suggested by Zwicky was the radius at which the total galaxy number density is twice that of the background. As pointed out by Peach and Beard (1969), this leads to systematic errors due to increasing background contamination for more distant clusters. Noonan (1972) has suggested the mean radius of cluster members as a size parameter for clusters. Austin and Peach (1974) find an inverse correlation between this parameter and core radius which they attribute to cluster evolution, and use a combination of the two to obtain a low dispersion.

To increase the power of the cluster angular size-redshift test, however, one needs many clusters to reduce the statistics. In the present paper we introduce a size parameter that is easy to measure, insensitive to cluster geometry, has a maximal signal to noise ratio over the background, a low dispersion, and may be applied to many clusters and to great distances.

Before applying this parameter to an angular size-redshift test, we need to know how it may be affected by evolution or other systematic effects. We have therefore undertaken a study of 64 cosmologically near clusters of galaxies in an attempt to gain an understanding

of the structural differences between various types of clusters, and how these differences may relate to evolution, and our size parameter. The selection of the sample and data reduction techniques are discussed in §II. The results of the analysis are presented in §III. The cluster sizes are first examined, then projected surface densities are determined and correlated with cluster type. The results are discussed in §IV.

II. THE DATA

Our study sample consists of almost all clusters with measured redshifts greater than $z = .0205$ and less than .1000, having declination $\delta > -30^{\circ}$ and galactic latitude $|b| > 15^{\circ}$. From the original sample, two clusters were omitted due to poor visibility on the plate, and five were rejected due to confusion from overlapping fields. The remaining 64 are listed in Table I. Column 1 gives the cluster name, columns 2 and 3 the 1950 coordinates, column 4 the galactic latitude, column 5 the cluster redshift, and column 6 the associated radio source if any.

All fields were photographed with the Palomar 48 inch Schmidt telescope on ten-inch plates. Kodak 098-04 emulsion was used behind 2 mm of RG-1 glass corresponding to the photographic F band (Oemler, 1974). The plates were

TABLE I

THE CLUSTERS STUDIED

(1) Cluster	(2) α	(3) β	(4) b	(5) z	(6) Radio
Zw499-13	0016	+2947	-32.3	.0226	
Zw478-5	0019	+2207	-40.0	.0207	
A76	0036	+0612	-56.3	.0377	
A119	0054	-0130	-64.1	.0446	3C29
A147	0106	+0126	-60.9	.0441	
0106+13	0106	+1304	-49.3	.0600	3C33
A151	0106	-1536	-77.6	.0526	
0117+31	0117	+3155	-30.3	.0591	4C31.04
A195	0126	+1842	-43.0	.0437	PKS0124+18
A272	0152	+3340	-27.1	.0877	
A278	0154	+3201	-28.6	.0904	
A376	0242	+3627	-20.8	.0487	
A400	0255	+0552	-44.9	.0231	
A407	0258	+3540	-20.0	.0473	
A465	0348	+0613	-35.2	.0855	
A505	0452	+7959	22.2	.0543	
A539	0513	+0555	-18.2	.0267	
A548	0546	-2534	-24.6	.0391	
A553	0608	+4841	-14.0	.0670	
A568	0705	+3506	18.4	.0779	
A576	0718	+5518	26.2	.0404	
A592	0740	+0930	15.6	.0621	
Zw118-3	0801	+2523	26.4	.0597	3C192
A634	0812	+5818	33.8	.0266	
Zw32-7	0820	+0647	23.3	.0809	3C198
A671	0825	+3037	33.0	.0497	
A754	0906	-0926	24.9	.0537	
A838	0935	-0449	33.2	.0507	
Zw211-58	1010	+3922	55.0	.0222	
A993	1019	-0440	41.6	.0530	
A1020	1024	+1039	52.1	.0650	
A1139	1055	+0147	52.6	.0376	
A1185	1107	+2852	67.5	.0349	
A1228	1118	+3422	69.3	.0344	
A1257	1124	+3538	70.2	.0339	

Table I (continued) The Clusters Studied

(1) Cluster	(2) α	(3) β	(4) b	(5) z	(6) Radio
A1314	1132	+4929	63.5	.0335	
A1377	1145	+5559	59.2	.0509	
Zw41-22	1215	+0400	65.2	.0766	MSH12+04
A1589	1239	+1852	81.2	.0718	
A1656	1257	+2814	88.0	.0230	
Zw160-23	1300	+3213	84.6	.0950	
1319+42	1319	+4251	73.4	.0797	3C285
A1736	1324	-2653	35.1	.0431	
A1775	1341	+2626	78.4	.0718	
1359-11	1359	-1128	47.6	.025	PKS1358-11
A1904	1420	+4837	62.4	.0719	
A1983	1450	+1657	60.2	.0458	3C306
A2048	1513	+0433	48.8	.0945	
A2052	1514	+0712	50.2	.0351	3C317
A2065	1520	+2754	56.7	.0722	
A2151	1603	+1755	44.5	.0360	
A2162	1610	+3000	46.2	.0318	
A2199	1627	+3939	43.7	.0312	
A2197	1628	+4055	43.5	.0303	
2059-28	2059	-2813	-39.6	.0379	PKS2058-28
Zw430-21	2247	+1107	-41.4	.0255	PKS2247+11
Zw430-10	2256	+1350	-40.5	.0331	3C455
Zw406-13	2308	+0720	-47.5	.0428	
A2593	2322	+1425	-43.2	.0440	
A2597	2323	-1224	-64.9	.0825	MSH23-112
A2634	2336	+2646	-33.1	.0307	3C465
A2657	2343	+0852	-50.4	.0414	
A2666	2348	+2652	-33.8	.0273	
A2670	2352	-1039	-68.5	.0753	

developed 8 minutes in MWP2.

Data reduction proceeded as follows. The plates were inspected visually, and the clusters identified. For each cluster, the brightest galaxies were selected for measurement. The number of galaxies selected per cluster ranged between 40 and 80 but was typically about 60. Galaxies were selected on the basis of their apparent luminosity as estimated visually, regardless of their position in the cluster. Galaxies closer to neighbouring clusters, and obvious foreground galaxies were excluded. Pairs of galaxies in apparent contact with one another were treated as single entities.

x-y coordinates of the selected galaxies were measured using a grid. Coordinates thus obtained were accurate to about .2 mm. From these coordinates, all possible separation vectors

$$\vec{r}_{ij} = \vec{r}_i - \vec{r}_j \qquad (1)$$

were constructed. These separations formed the basic set of data defining each cluster. They preserve many structural properties of the cluster, but contain no direct reference to spatial features such as the location of the cluster center. Moreover, irregular clusters may be treated in the same manner as symmetric clusters. Concepts such as the central density are replaced by the "maximum local density". Physically, the spectrum of separations to nearby

galaxies is of greater consequence to a galaxy than its particular location in a cluster as it is these separations that determine the gravitational forces on the galaxy.

III. RESULTS

a) The Cluster Types

Rood and Sastry (1971) have devised a classification scheme for clusters of galaxies based on the appearance of the cluster. Forty one of our clusters are included in their published classifications. The remainder were classified according to their appearance on our plates following the type definitions outlined by Rood and Sastry. Generally speaking, cD clusters are clusters containing a supergiant (cD) galaxy (Morgan and Lesh, 1965). B clusters contain two giant galaxies; the Coma cluster is a well known example. L clusters contain a linear arrangement of the brightest galaxies and C clusters contain a concentration of the brighter members in a core-halo type configuration. F clusters display an overall flattening, and I clusters are irregular. The types for all our clusters are listed in column 2 of Table II. The distribution of types in our sample is shown in Figure 1. Irregular clusters predominate followed by a large number of core-halo types. Fourteen percent of our clusters contain cD galaxies. About one

TABLE II

THE CLUSTER PARAMETERS

(1) Cluster	(2) RS Type	(3) $\log\lambda_c$	(4) $\log\lambda_h$	(5) log C	(6) log K	(7) N
Zw299-13	C	-.009	.343	.352	.373	51
Zw478-5	C	.009	.357	.348	.321	52
A76	L	-.075	.171	.246	.316	50
A119	C	.085	.352	.269	.659	54
A147	I	.219	.514	.295	.344	63
0106+13	cD	.084	.324	.240	.246	64
A151	cDp	.107	.359	.252	.317	78
0117+31	I	.094	.391	.297	.475	79
A195	L	.181	.493	.312	.353	54
A272	I	-.090	.181	.271	.315	48
A278	I	-.033	.200	.233	.220	49
A376	I	.106	.426	.320	.338	48
A400	I	-.076	.251	.327	.749	57
A407	C	-.062	.260	.322	.525	58
A465	F	.036	.271	.235	.282	57
A505	cD	-.009	.210	.219	.171	51
A539	F	-.079	.225	.304	.446	61
A548	F	.002	.228	.226	.275	66
A553	I	.011	.256	.245	.248	50
A568	C	-.024	.301	.325	.547	56
A576	I	.208	.559	.351	.796	57
A592	F	.195	.468	.273	.484	64
Zw118-3	I	.135	.453	.318	.690	56
A634	F	.078	.349	.271	.403	51
Zw32-7	F	.307	.606	.299	.547	54
A671	C	.126	.436	.310	.306	61
A754	cD	.002	.261	.259	.247	67
A838	Bb	.138	.413	.275	.336	58
Zw211-58	C	-.177	.168	.345	.379	47
A993	I	.141	.434	.293	.355	68
A1020	L	.177	.430	.253	.326	57
A1139	I	.019	.293	.274	.378	61
A1185	C	.052	.458	.406	.694	62
A1228	I	.112	.374	.262	.467	67
A1257	L	.136	.374	.238	.306	68

Table II (continued) The Cluster Parameters

(1) Cluster	(2) RS Type	(3) $\log\lambda_c$	(4) $\log\lambda_h$	(5) log C	(6) log K	(7) N
A1314	C	-.032	.283	.315	.292	53
A1377	B	-.129	.179	.307	.423	76
Zw41-22	L	.050	.278	.228	.238	65
A1589	C	.192	.503	.311	.296	67
A1656	B	.078	.383	.305	.268	71
Zw160-23	F	-.004	.280	.284	.325	64
1319+42	I	.055	.299	.244	.332	63
A1736	I	.100	.388	.288	.417	76
A1775	B	.126	.383	.257	.445	52
1359-11	I	.236	.585	.349	.339	56
A1904	Bb	.086	.444	.358	.528	73
A1983	F	-.032	.235	.267	.215	56
A2048	C	.022	.254	.232	.227	57
A2052	cD	-.059	.189	.248	.551	40
A2065	C	-.126	.175	.301	.345	68
A2151	F	.019	.244	.225	.275	74
A2162	I	.321	.604	.283	.243	45
A2199	cDp	.149	.382	.233	.230	48
A2197	L	.116	.314	.198	.159	53
2059-28	I	-.053	.161	.214	.203	46
Zw430-21	B	.173	.394	.221	.272	50
Zw430-10	F	.155	.445	.290	.171	42
Zw406-13	C	.052	.281	.229	.230	50
A2593	Ip	.331	.654	.314	.636	75
A2597	L	.046	.276	.230	.208	60
A2634	cD	.201	.465	.264	.367	60
A2657	F	.113	.443	.330	.618	73
A2666	cDp	.117	.378	.261	.304	47
A2670	cD	-.025	.221	.246	.285	66

FIGURE 1

Distribution of clusters by Rood and Sastry type classification.

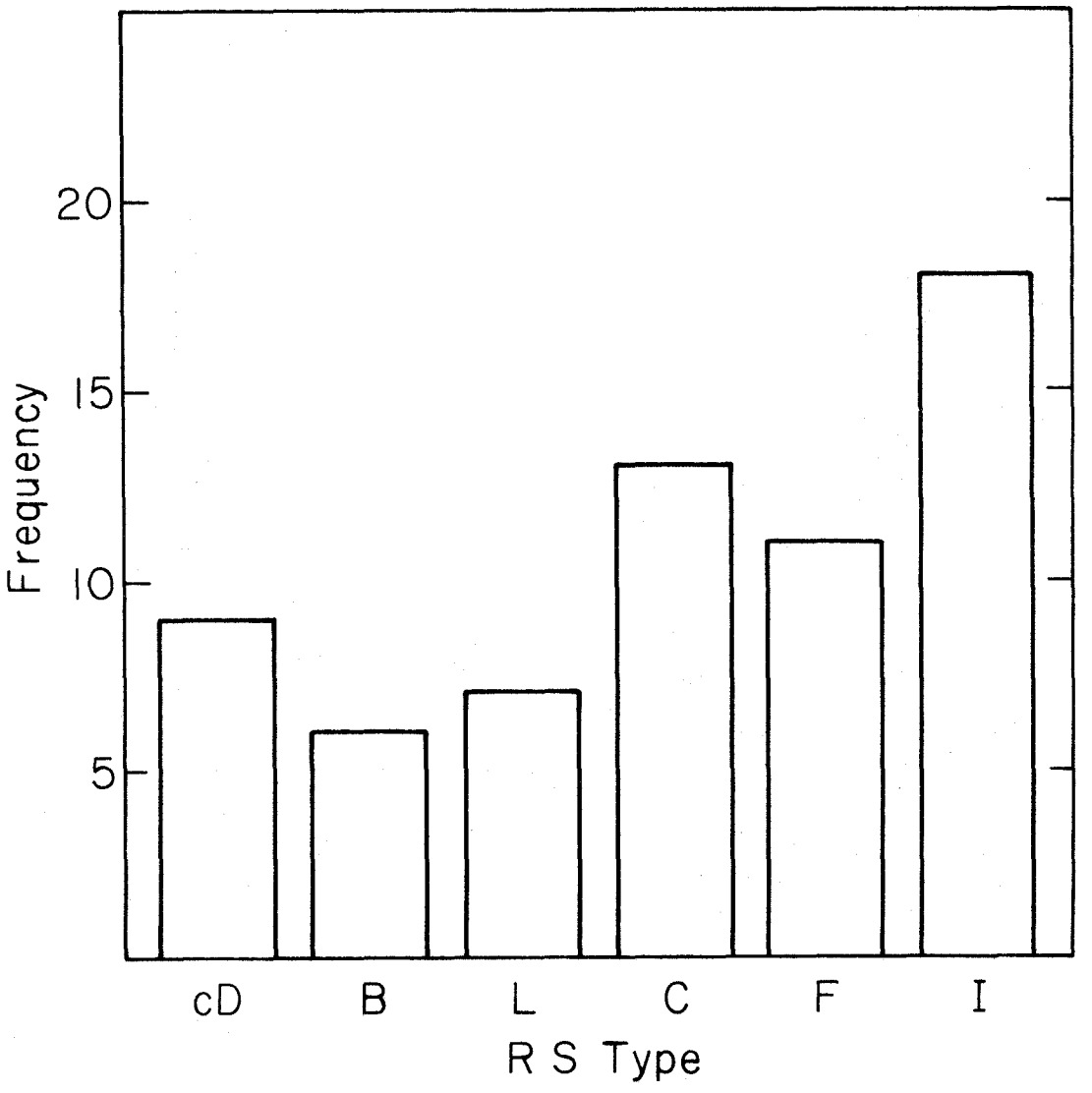
20
15
10
5
Frequency
cD
B
L
C
F
I
R S Type

quarter of our sample contains one or more giant galaxies.

b) The Cluster Sizes

From the separations $\vec{r}_{ij}$ we compute the "core" size λ_c of a cluster from the definition

$$\lambda_c \equiv \left\{ \frac{2}{N(N-1)} \sum_{i>j}^{N} \frac{1}{r_{ij}} \right\}^{-1} , \quad r_{ij} = |\vec{r}_{ij}| \tag{2}$$

and the "halo" size

$$\lambda_h \equiv \frac{2}{N(N-1)} \sum_{i>j}^{N} r_{ij} \tag{3}$$

where N is the number of galaxies selected in the cluster. Following Austin and Peach (1974) we define a "concentration factor"

$$C \equiv \lambda_h / \lambda_c \tag{4}$$

which measures the degree of core-halo separation. Also of interest is the "clumpiness" defined here as

$$K \equiv \frac{1}{\lambda_c} \left\{ \frac{2}{N(N-1)} \sum_{i>j}^{N} \frac{1}{r_{ij}^2} \right\}^{-\frac{1}{2}} \tag{5}$$

The resulting values are listed in column 3, 4, 5, and 6 of Table II. The number of galaxies counted in each cluster is listed in column 7.

Any systematic relations between the size parameters and cluster types are of considerable importance to the angular size-redshift test, and to an understanding of cluster evolution in general. In Figure 2 the structure parameters are shown averaged over the cluster types. The bars extend one standard deviation above and below the mean values. The standard deviation of the mean is indicated by the shaded portion. The numerical values are tabulated in Table III. The most significant effect we observe, is that the sizes of the clusters are remarkably constant, regardless of cluster type. All clusters, from the irregulars to the cD clusters, display nearly the same sizes. Formally the core radius λ_c has the lowest standard deviation. It is also less sensitive to the outer regions of the cluster where the signal to noise (field galaxies) ratio is poor. Thus it would probably be the best statistic for cosmology.

The core size for C type clusters falls about two standard deviations below the mean. This results from small subgroups of galaxies that affect the core size more strongly than the halo size which is normal. This shows up as high values for the concentration and clumpiness parameters.

Another pronounced effect here is the very low dispersion and mean value of the concentration parameter for cD clusters. These clusters are uniformly smooth, with little

FIGURE 2

Structure parameters for various cluster types. The bars extend one standard deviation above and below the mean values. The standard deviation of the mean is indicated by the shaded portion.

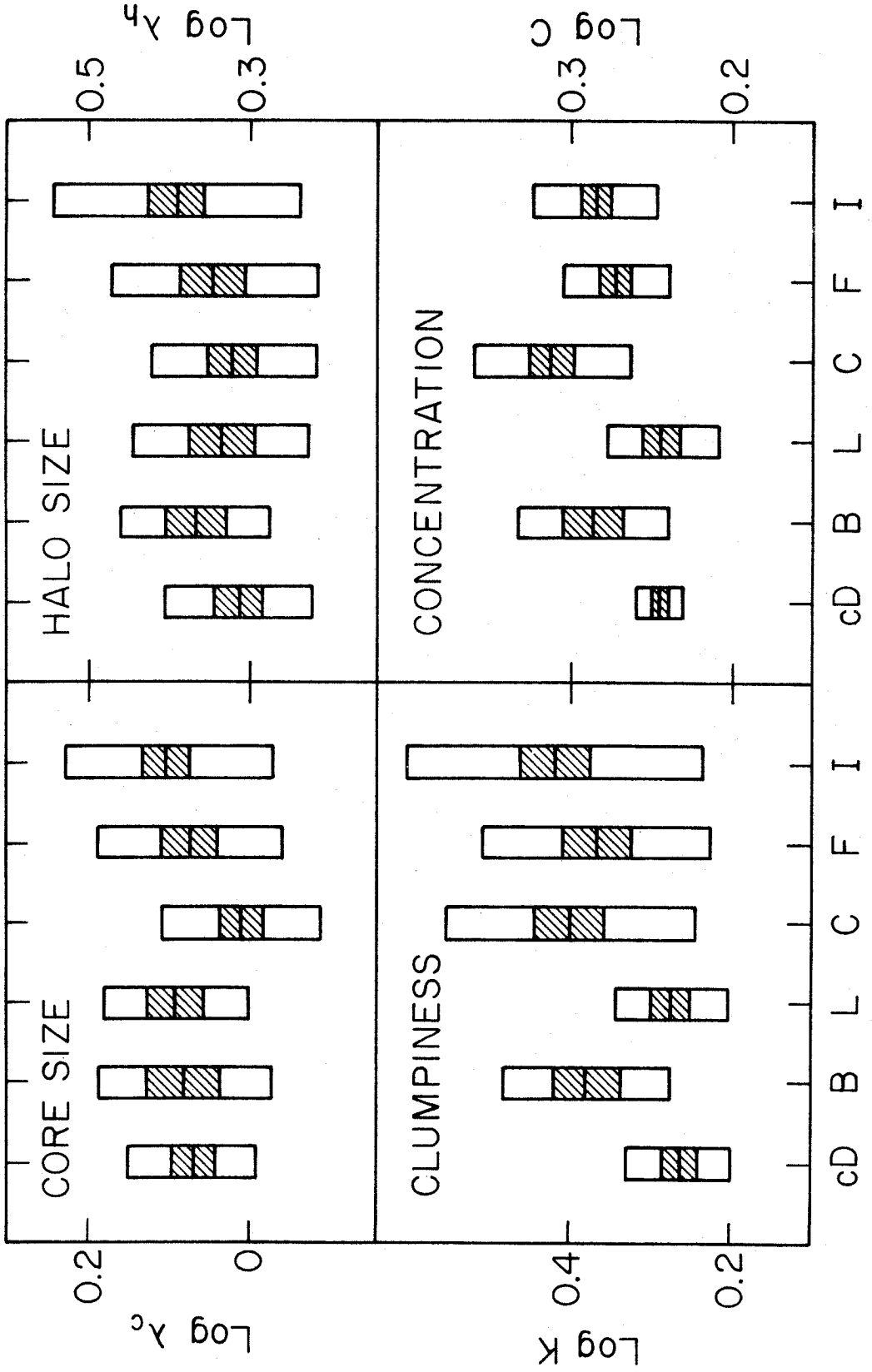
Log λ_h
0.5
0.3
HALO SIZE
Log C
0.3
0.2
CONCENTRATION
cD B L C F I
Log λ_c
0.2
0
CORE SIZE
Log K
0.4
0.2
CLUMPINESS
cD B L C F I

TABLE III

MEAN VALUES OF CLUSTER PARAMETERS

Parameter	RS Type cD	B	L	C	F	I	All
$<\log\lambda_c>$	.067	.079	.090	.008	.072	.102	.069
$\sigma_{\log\lambda_c}$	.083	.108	.091	.099	.113	.127	.109
$\sigma_{<\log\lambda_c>}$	.028	.044	.034	.027	.034	.030	.014
$<\log\lambda_h>$	.312	.366	.334	.321	.345	.390	.349
$\sigma_{\log\lambda_h}$	.091	.094	.108	.102	.128	.151	.121
$\sigma_{<\log\lambda_h>}$	.030	.038	.041	.028	.039	.036	.015
<log C>	.245	.287	.244	.313	.273	.286	.279
$\sigma_{\log C}$	.015	.047	.035	.049	.034	.039	.039
$\sigma_{<\log C>}$	.005	.019	.013	.014	.010	.009	.005
<log K>	.261	.379	.272	.400	.367	.419	.364
$\sigma_{\log K}$	.064	.104	.071	.156	.143	.183	.141
$\sigma_{<\log K>}$	.021	.042	.027	.043	.043	.043	.018

tendency towards clumping of the galaxies. B clusters, surprisingly do not show this effect, but appear to be more like C clusters in clumpiness and concentration. L clusters also show low values of these parameters, like the cD clusters.

In Figure 3 we have plotted concentration against cluster core size. There is a general tendency particularly among the F and I type clusters for clusters with larger core size to have larger values of C, i.e., relatively larger halos. The figure suggests the approximate relation

$$\lambda_c \sim \lambda_h^{\frac{3}{4}} \tag{6}$$

The upper left corner of Figure 3 is occupied primarily by C type clusters. This is a result of small knots of galaxies in these clusters that simultaneously decrease the core size, and increase the concentration.

Since the number of galaxies (N) counted per cluster was not fixed, we must check for any dependence of the sizes on N. Counting different numbers of galaxies in the same cluster would be inconclusive because of statistical fluctuations. Instead we group the clusters into bins according to the number of galaxies counted, and average the cluster sizes in each bin. The results are shown in Figure 4 where we plot the mean values. The error bars indicate the standard deviations of the means. It is apparent that there is little systematic effect, if any, between the

FIGURE 3

The cluster concentration $C = \lambda_h/\lambda_c$ is plotted against the core size λ_c for the 64 clusters in our sample. Symbols indicate cluster type according to the type designations of Rood and Sastry.

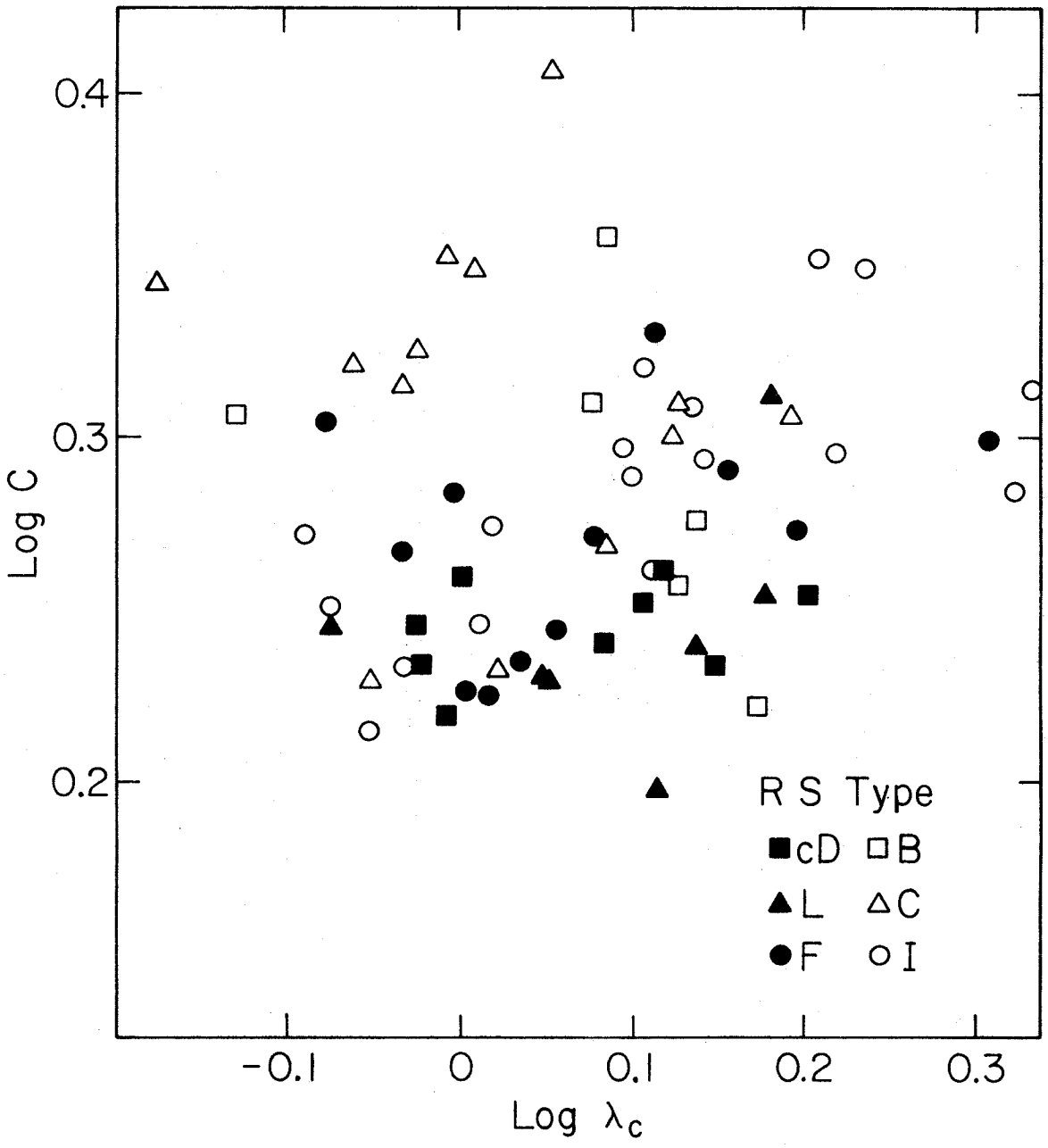
0.4
0.3
0.2
Log C
-0.1
0
0.1
0.2
0.3
Log λ_c
R S Type
cD
B
L
C
F
I

FIGURE 4

Mean values of the core size λ_c are plotted for ranges of the number of galaxies counted. Error bars indicate the standard deviations of the means.

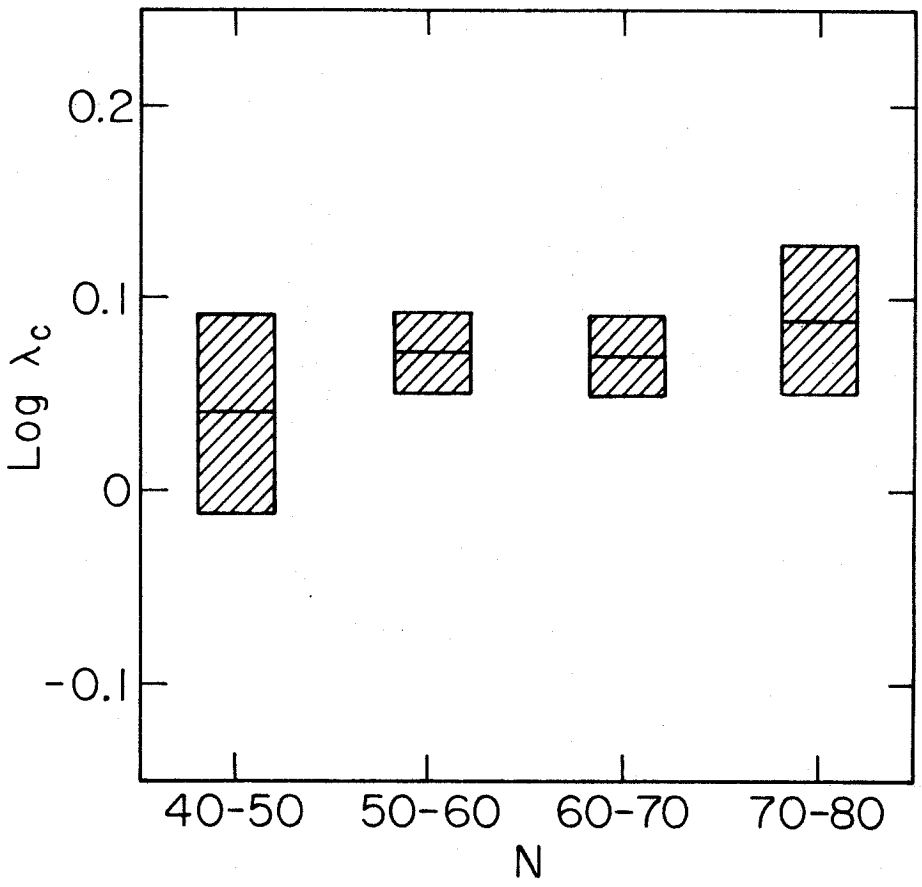
0.2
0.1
0
-0.1
Log λ_c
40-50
50-60
60-70
70-80
N

cluster sizes and the number of galaxies counted, within this range.

c) The Cluster Profiles

The lack of symmetry of most clusters makes radial surface density profiles difficult to determine, if they can be meaningfully defined. A profile that arises natuarally from the galaxy positions is the distribution of intergalactic separations. This is a well determined function for all types of clusters, and there are no fitting parameters such as the location of the "center" of the cluster. Since the number of intergalactic separations between two small regions of a cluster is proportional to the product of the number of galaxies in each region, it follows that the distribution of separations is given by the autocorrelation function of the surface density distribution.

$$p(\vec{r}) = \sigma(\vec{r}) * \sigma(\vec{r}) \tag{7}$$

Thus we can obtain a relation between the distribution of separations and the radial surface density distribution of a cluster. If the number of separations in the range (s, s + ds) is P(s) we have

$$P(s) = 4\pi s \int_0^{\pi} \int_0^{\infty} \sigma(r)\,\sigma\left(\left[r^2+s^2-2rs\cos\theta\right]^{\frac{1}{2}}\right) r\,dr\,d\theta \tag{8}$$

The observed profiles are plotted in Figure 5, for various cluster types. The cluster sizes have been scaled by the size parameter λ_h, as measured for each cluster. Since the number of galaxies counted per cluster was not constant, the profiles are normalized to unit area.

The cD clusters show a fairly well defined mean profile. By means of equation (8) we have fit an exponential surface density distribution to the data, as shown by the dashed line in Figure 5. We find the relation

$$\sigma(r) \sim e^{-\frac{r}{r_o}}$$

where

$$\begin{aligned} r_o &\simeq .37\ \lambda_h \\ &\simeq .64\ \lambda_c \end{aligned} \tag{9}$$

provides a good fit to the data for these clusters. The mean value of r_o for our cD clusters is

$$\langle r_o \rangle = .75\ \text{Mpc} \pm 20\% \tag{10}$$

The cD clusters that deviated the most from this profile were those that had been classified by Rood and Sastry as cDp due to the main body of the cD galaxy being multiple or otherwise peculiar. These tended to have a small dip in the profile near its maximum. The most outstanding deviant, Abell 2666, is shown by the open circles in Figure 5. It is deficient in separations of about 1 Mpc and shows an excess at about 2 Mpc. The cluster itself lacks the uniformity of the other cD clusters, and divides generally into two main groups of galaxies, one containing the cD galaxy which has

FIGURE 5

The cluster profiles. The distribution of intergalactic separations is shown for various cluster types. The dashed line superimposed on the cD cluster distribution results from an exponential surface density (projected) distribution. The open circles correspond to the cluster Abell 2666

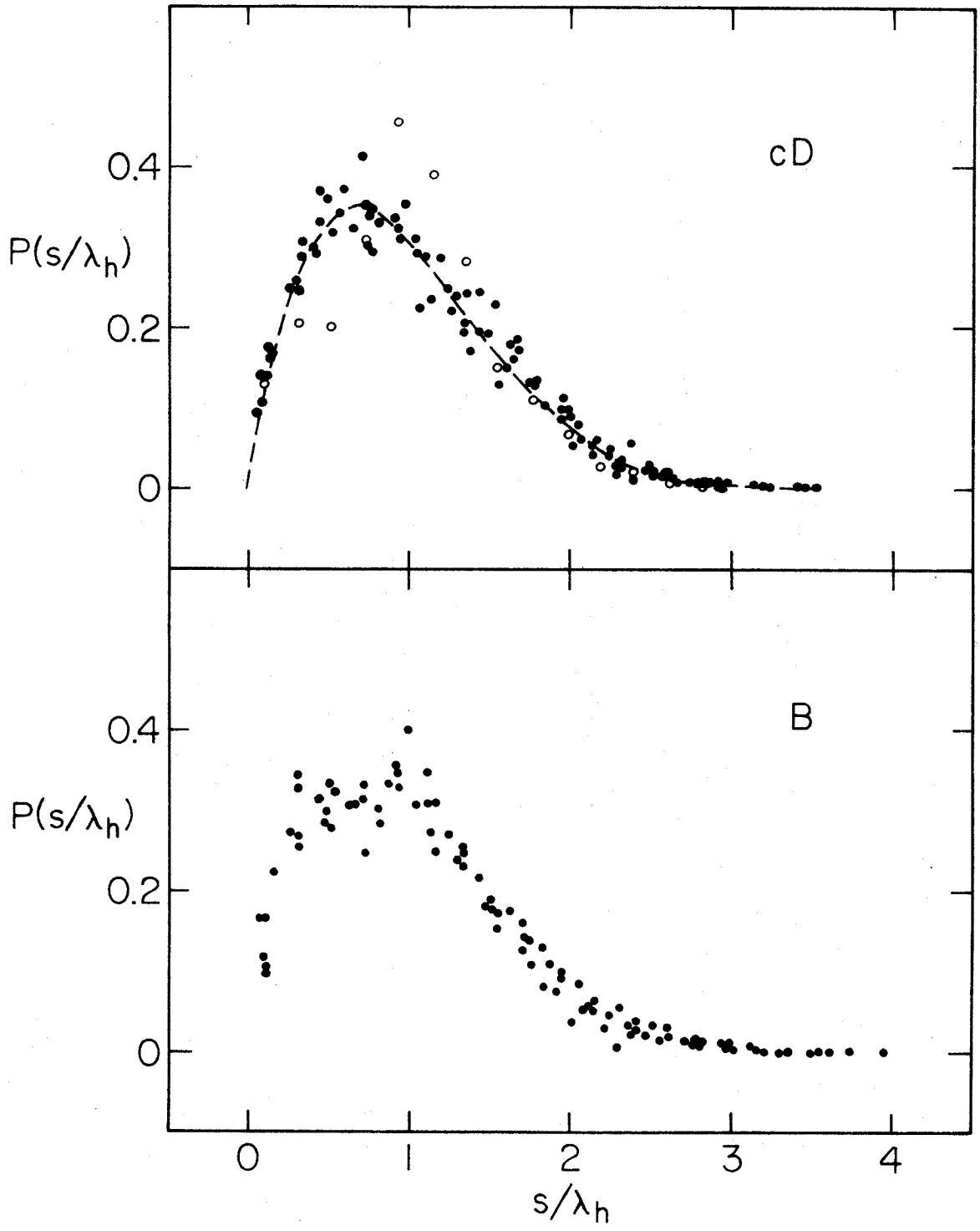
cD
B
0.4
0.2
0
P(s/λh)
0
1
2
3
4
s/λh

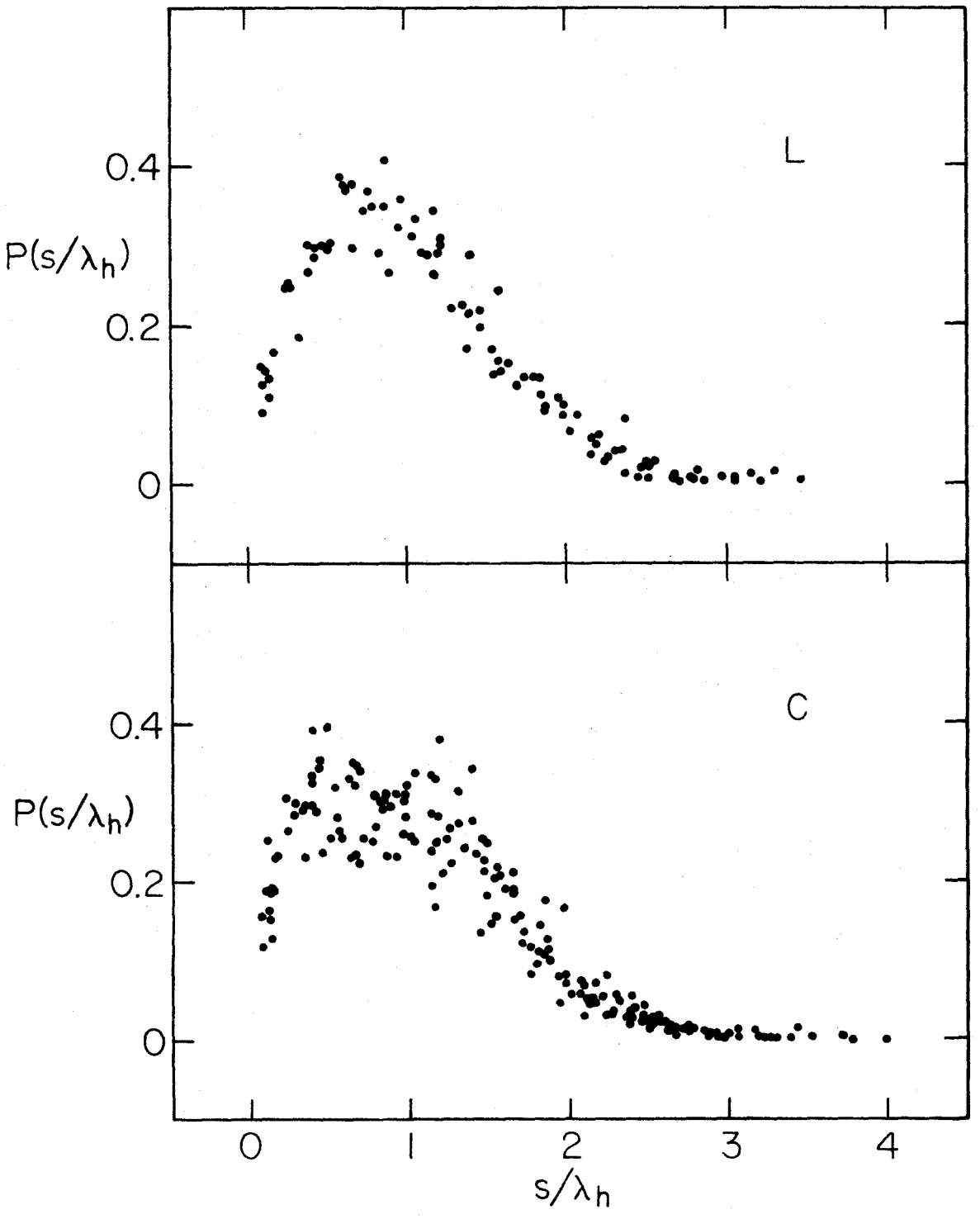
L
C
0.4
0.2
0
P(s/λh)
0
1
2
3
4
s/λh

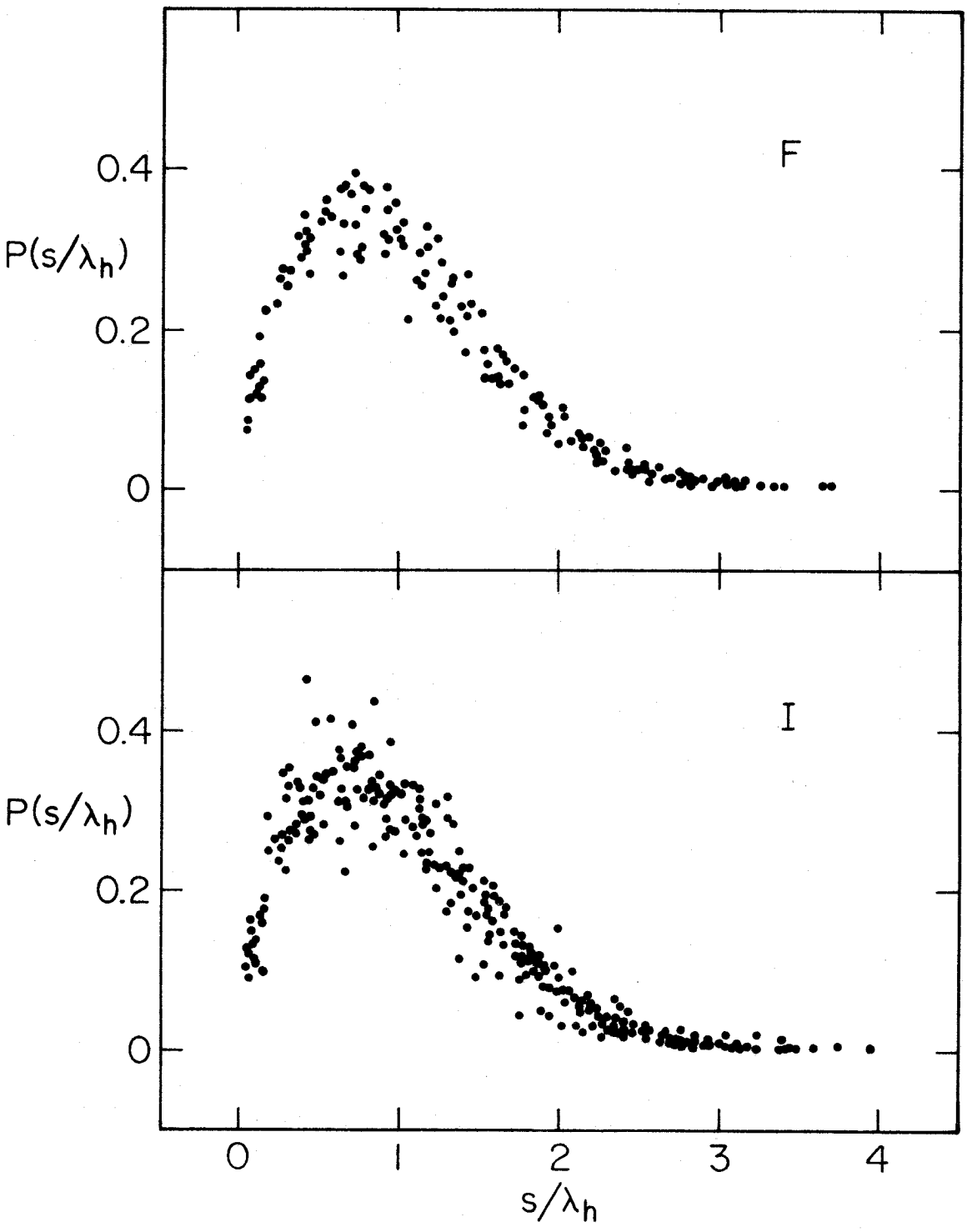
F
I
0.4
0.2
0
P(s/λh)
0
1
2
3
4
s/λh

a small object adjacent to its nucleus, and shows some structure in its outer envelope.

The B cluster profiles differed significantly from those of the cD cluster. While the overall shape is the same, most clusters show a distinct local minimum in the number of separations between 1 and 2 Mpc. This may be related to the feature observed in the luminosity profile of rich clusters (Bahcall, 1971, Clark, 1968, Oemler, 1974). However we find it to be less evident in cD clusters, but strong in B and C types. Spatially it corresponds to a core-halo type separation in the cluster, i.e., a two component picture in which one or more relatively compact condensations appear in a more tenuous envelope of galaxies.

The L and F profiles were very similar to those of the cD clusters. The F distribution, however, tended to peak at slightly larger relative separations indicating a slight deficiency of small separations relative to the L and cD clusters. The I cluster profiles tended to be somewhat more irregular, but conformed, on the average, to the same general distribution as the F clusters.

IV. DISCUSSION

The result that we would most like to emphasize here is that clusters contain an intrinsic size parameter which shows relatively little dispersion over a wide range of cluster types and classes, yet can be easily measured from the positions of relatively few bright galaxies. The measured sizes λ_c and λ_h can be directly related to an intrinsic scale size r_o describing the distribution of the brighter galaxies. The low dispersion in the core size λ_c is partly due to the fact that large, irregular clusters contain relatively dense clumps of galaxies that tend to offset the larger separations between the clumps. Clusters that appear relaxed have a more uniform spacing of galaxies (i.e., lower values of C and K), which tends to offset the fact that their cores are smaller.

Considering the nature of the selection criteria for these clusters, it seems likely that they provide a fair sampling of cluster evolutionary types. The irregular clusters are probably in the pre-collapse phase, but may contain local bound condensations that have collapsed sooner due to their higher density. cD clusters have almost certainly completely collapsed and are near equilibrium (with the possible exception of clusters like A2666), as the they display a high degree of regularity in their

structure parameters. The situation regarding Abell 2666 is unclear. It may be that cD galaxies form from collisions (Ostriker and Tremaine, 1975) in a dense core of galaxies before all of the cluster has had time to relax. This would account for the association between peculiar looking cD galaxies and the irregularities in the cluster profiles, as older, more relaxed clusters would contain cD galaxies that would have had time to distribute their component material more evenly.

REFERENCES

Austin, T. B., and Peach, J. V. 1974, M.N.R.A.S., 167, 437.

Bahcall, N. A. 1971, Ap.J., 76, 995.

———. 1975, Ap.J., 198, 249.

Clarke, E. E. 1968, Ap.J., 73, 1011.

Morgan, W. W., and Lesh, J. R. 1965, Ap.J., 142, 1364.

Noonan, T. W. 1972, A.J., 77, 134.

Oemler, A. 1974, Ap.J., 194, 1.

Ostriker, J. P., and Tremaine, S. D. 1975, Ap.J. (Letters), 202, L13.

Peach, J. V., and Beard, J. M. 1969, Ap. Letters, 4, 205.

Rood, H. J., and Sastry, G. N. 1971, P.A.S.P., 83, 313.

Sandage, A. 1961, Ap.J., 133, 355.

Zwicky, F. 1957, Morphological Astronomy, (Berlin: Springer Verlag).

I. INTRODUCTION

Direct observational determinations of the deceleration parameter q_o have generally been by means of the magnitude redshift test (Sandage, 1961, Sandage and Hardy, 1973, Gunn and Oke, 1975). However the evolutionary correction to the magnitudes of the brightest cluster galaxies remains uncertain. It is therefore desirable to have as many different approaches to the problem as possible. The concept of using clusters of galaxies in an angular size-redshift test was considered by Zwicky (1957) who suggested an isothermal core radius as a suitable size parameter for rich clusters. This approach has been recently applied by several authors (Peach and Beard, 1969, Austin and Peach, 1974, Bahcall, 1975). Other size parameters have been investigated (de Vaucoulers, 1948, Noonan, 1972, King, 1972) and applied to rich clusters. Statistical uncertainties however remain large. This motivated us in Part I to investigate the spatial structure of a relatively large sample of clusters to search for a size parameter that could be easily applied to all types of clusters with a minimum of systematic and statistical errors. Such a parameter was found, and in the present paper we use a slightly modified version of it in an angular size-redshift test with 95 clusters of galaxies.

The angular size red-shift test is developed in §II. Our

size parameter and its statistics are discussed in §II a. In §II b we consider the contaminating effects of field galaxies on the value of the size parameter and its accuracy. Our definition of the cluster size leads to a systematic effect similar to the "aperture effect" of the magnitude-redshift test. This effect is investigated in §II c with the help of Monte Carlo type numerical simulations. In combination with the field galaxy contamination (background effect) we develop an iterative technique to remove both effects from the data. At this point we can predict the accuracy of the method for determining q_o. The data for our study is presented in §III and the reduction techniques described in §IV. Our results are given and discussed in §V. Evolutionary corrections are considered in §VI and a "corrected" value of q_o is determined. An upper limit is found for possible evolutionary effects on q_o. In §VII we discuss the accuracy and reliability of the test, and propose a way of extending it to greater distances.

II. THE TEST

a) The Size Parameter

In Part I we found that the harmonic mean separation of the brightest galaxies in a cluster was a remarkably constant statistic. We now wish to develop this into a size parameter suitable for cosmological investigations.

Although the results of Part I indicated little correlation between the harmonic mean separation and the number of galaxies measured (within the range of the data) we choose to fix the number of galaxies so as to eliminate any possible systematic error from this source. In view of the poor visibility of distant clusters we adopt 40 as the number of galaxies measured per cluster.

An important systematic effect arises due to the decreasing visibility of clusters with increasing distance. As was pointed out by Peach and Beard (1969), in connection with Zwicky (1961-1968) sizes of clusters, distant clusters will appear smaller when measured to a given level of contrast or visibility above the background (field galaxies). Rather than be influenced by this effect when estimating cluster membership, we adopt the procedure of measuring all eligible galaxies within a circle of constant metric radius centered on the cluster (eligible here means being among the 40 brightest galaxies not brighter than the brightest cluster galaxy). The angular size of the circle depends on the cosmological model. This gives rise to an aperture effect (discussed in §VI) which decreases the power of the method. We would rather accept this however, than introduce a poorly determined systematic error into the test. We choose an angular size corresponding to a metric radius of 3 Mpc in an empty pressureless Friedmann universe with zero

cosmological constant, and $q_o = 0$.

We thus define the cluster size as the harmonic mean (projected) separation between the 40 brightest (not exceeding the brightest cluster galaxy) galaxies within a circle of 3 Mpc radius ($q_o = 0$) centered on the cluster:

$$\lambda = \left\{ \frac{2}{N(N-1)} \sum_{i>j}^{N} \frac{1}{s_{ij}} \right\}^{-1} \tag{1}$$

where s_{ij} is the projected separation between the ith and jth galaxy in Mpc ($q_o = 0$), and N = 40.

Let us estimate the errors associated with this parameter. We measure N(N - 1)/2 separations between N galaxies. However, only 2N - 3 of these may be considered statistically independent. In practice we use all separations to determine λ. This has little effect on the errors, so for the purpose of the present discussion, we consider only the independent separations.

If the number of separations in the range s + ds is P(s) we have:

$$\lambda^{-1} = \frac{1}{M} \sum_{i=0}^{M} \frac{1}{s_i} P(s_i) \equiv \left\langle \frac{1}{s} \right\rangle \quad , \quad M = 2N-3$$

$$\therefore \quad \mathrm{Var}\, \lambda^{-1} = \frac{1}{M^2} \sum_i \frac{1}{s_i^2} \mathrm{Var}\, P(s_i) = \frac{1}{M^2} \sum_i \frac{1}{s_i^2} P(s_i) = \frac{1}{M} \left\langle \frac{1}{s^2} \right\rangle \tag{2}$$

Thus we estimate the uncertainty in $\ln\lambda$ to be on the order

of

$$\sigma_{\ln\lambda} \simeq \frac{1}{\sqrt{(2N-3)}} \frac{\left\langle \frac{1}{s^2} \right\rangle}{\left\langle \frac{1}{s} \right\rangle} \equiv \frac{K}{\sqrt{(2N-3)}} \qquad (3)$$

Numerical cluster simulations (described in §II c) give a mean value of 1.6 for the clumpiness K. Taking N = 40 gives for our estimated uncertainty;

$$\sigma_{\ln\lambda} \simeq .18 \qquad (4)$$

This error is consistent with standard deviations found in the numerical simulations. In the above analysis we have assumed that all the points are from the same distribution, i.e., there are no field galaxies contaminating the sample. We now consider the effects of field galaxies on the cluster size and its uncertainty.

b) Field Galaxies

It is of utmost importance that the effects of field galaxies be properly accounted for as they affect the cluster sizes systematically. We assume that the number N_f of field galaxies in our sample can be estimated by an analysis of the sky surrounding the cluster. The details of the actual method used are discussed in §V.

To proceed further, it is necessary to assume something about the distribution of the field galaxies in the aperture.

In general both foreground and background galaxies will be present, both isolated and as members of other clusters. Clusters showing obvious overlapping are rejected from the study group. For those remaining we shall assume that the field galaxies are distributed randomly over the aperture.

The degree to which field galaxies affect the measured cluster size depends on several factors such as the number of field galaxies, the "intrinsic" size of the cluster, and the cutoff radius of the aperture (which is in itself a function of q_o). Due to the complexity of the effect, the correction has been computed from the numerical cluster simulations described in §IV. The results are shown in Figure 1. With increasing background, the measured cluster size increases at a rate determined by the ratio of the "intrinsic" cluster size to the cutoff radius.

Background galaxies also decrease the sensitivity of the test. The effect is twofold: Due to the inclusion of N_f field galaxies in the sample, we have only $N_c = 40 - N_f$ cluster galaxies from which to estimate the cluster size which gives a larger statistical uncertainty. Also the statistics of the field galaxies contributes additional uncertainty to our calculated size λ. The magnitude of the effect may be estimated as follows: For N_f field galaxies there are $2N_c - 3$ independent separations containing information about the cluster, where $N_c + N_f = 40$.

FIGURE I

Effect of field galaxy contamination on the measured cluster sizes.

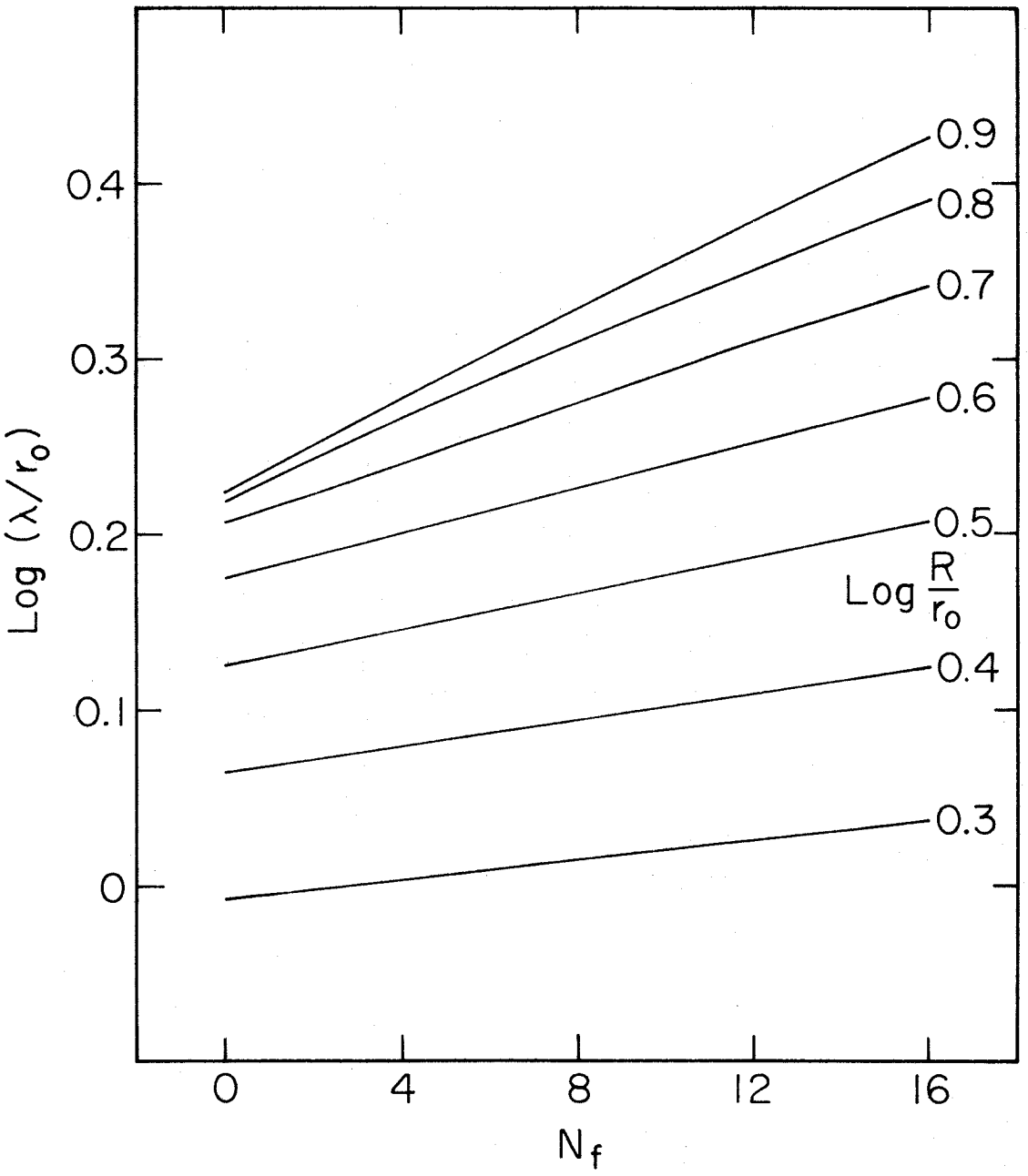
0.9
0.8
0.7
0.6
0.5
0.4
0.3
Log R/r₀
0.4
0.3
0.2
0.1
0
Log (λ/r₀)
0
4
8
12
16
N_f

Thus there remain $2N - 3 - (2N_c - 3) = 2N_f$ independent separations contributing only "noise". So

$$\mathrm{Var}\left\{(2N_c-3)\,\lambda^{-1}\right\} = \sum_{i=0}^{2N_c-3} \frac{1}{s_i^2} P_c(s) + \sum_{i=0}^{2N_f} \frac{1}{s_i^2} P_f(s)$$

$$= (2N_c-3)^2 \ \mathrm{Var}\,\lambda^{-1}$$

$$\therefore \qquad \mathrm{Var}\,\lambda^{-1} = \frac{1}{2N_c-3}\left\langle\frac{1}{s^2}\right\rangle_c + \frac{2N_f}{(2N_c-3)^2}\left\langle\frac{1}{s^2}\right\rangle_f \qquad (5)$$

Setting $\varepsilon = N_f/N_c$ we obtain

$$\mathrm{Var}\,\lambda^{-1} \simeq \frac{1}{2N-3}\left\{(1+\varepsilon)\left\langle\frac{1}{s^2}\right\rangle_c + \varepsilon(1+\varepsilon)\left\langle\frac{1}{s^2}\right\rangle_f\right\}$$

$$\therefore \qquad \sigma_{\ln\lambda} \simeq \frac{K_c}{\sqrt{(2N-3)}}\left\{(1+\varepsilon)^{\frac{1}{2}}\left[1+\varepsilon\left(\frac{K_f}{K_c}\right)^2\right]^{\frac{1}{2}}\right\} \qquad (6)$$

The error has been increased by the factor in parenthesis which for $K_f \simeq K_c$ becomes $1 + \varepsilon$. Taking $N_f = 14$ as our worst case gives an increase in uncertainty by a factor 1.5 over an uncontaminated cluster.

c) The Aperture Effect

For reasons already discussed, a fixed cutoff radius was introduced into the definition of the cluster size. Since this requires a knowledge of q_o, negative feedback is introduced which decreases the sensitivity of the test. The effect is analagous to the aperture correction of the magnitude-redshift test (see Gunn and Oke, 1975 for a complete discussion).

If q_o is not zero, the cutoff will not occur at the same metric radius for all clusters, so the values of λ will be systematically in error. In our case, however, the magnitude of the error for any particular cluster depends not only on the value of q_o, but also on the "intrinsic" cluster size, and the number of field galaxies in the sample. To analyze these effects we have constructed a sequence of Monte Carlo type computer simulations of clusters of galaxies. Clusters are represented by 40 points, N_c of which are distributed by an exponential projected surface density with scale factor r_o (the "intrinsic" cluster size) and cutoff radius R_c. The remaining N_f points are distributed at random within the circle defined by the cutoff radius R_c. An exponential distribution was chosen for the cluster because it conforms well to the observed profiles of the cluster studied in Part I.

Models were calculated for a range of values of N_f and

$\zeta \equiv \log(r_o/R_c)$. For each pair of values (N_f, ζ) twenty-five statistical realizations of the cluster were analyzed and the resulting values of λ averaged. The statistical dispersion in $\log\lambda$ averaged about .05. The results of the models appear in Figure 2. To remove statistical fluctuations, and to make the results manageble, the data has been fit with the following equation:

$$\log(\lambda/r_o) = \frac{\mu\zeta}{\left(\frac{R_c}{r_o}\right)^{\nu} + \mu} + \gamma$$

where

$$\nu = \frac{5}{4} \quad , \quad \mu = 4.24\,\frac{\epsilon}{\sqrt{(1+\epsilon)}} + 15.9$$

$$\gamma = .016\,\epsilon\,(1+\epsilon^2) - .268 \quad , \quad \epsilon = \frac{N_f}{40 - N_f} \qquad (7)$$

Equation (7) is the result of an eyeball fit to the data and is taken to be representative of the underlying distribution governing these variables within the range of these models. For any given R_c (from the cosmological model being tested) and measured λ and N_f, the "intrinsic" size r_o may be determined iteratively from equation (7) This equation may then be reapplied to give the corrected or "standard" size λ_r by using R_c = 3 Mpc, N_f = 0, and taking

FIGURE 2

The aperture correction. The ratio of measured to intrinsic size is plotted versus cutoff radius and field galaxy content.

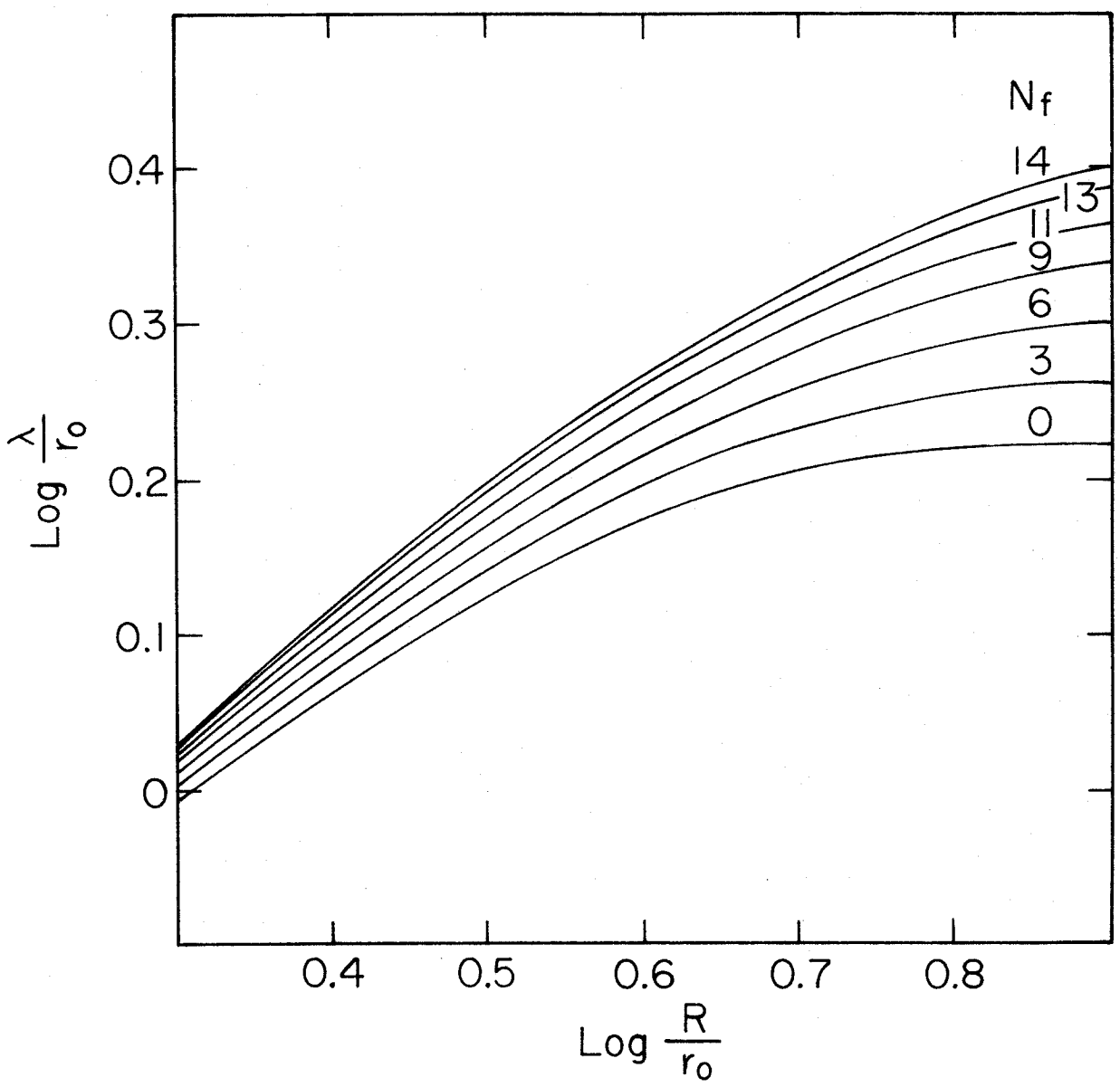
N_f
14
13
11
9
6
3
0
0.4
0.3
0.2
0.1
0
$\text{Log } \frac{\lambda}{r_o}$
0.4
0.5
0.6
0.7
0.8
$\text{Log } \frac{R}{r_o}$

r_o from the iterative calculation.

III. THE DATA

A study sample of clusters for this test was selected according to the following criteria:

1. The clusters all had measured redshifts $z > .0205$.
2. The clusters were north of $\delta = -30^o$.
3. The clusters had galactic latitude $|b| > 15^o$.

Clusters with redshifts less than $z = .1$ were photographed with limiting exposures on 10 inch 098-04 plates behind 2mm RG-1 glass on the 48 inch Schimidt telescope at Palomar. Kodak type 127-02 plates, baked nine hours in N_2 at 65^oC were used to record clusters of redshift $z = .1$ or greater. Again limiting exposures with the RG-1 filter were employed.

Of the original sample, five clusters were rejected because of uncertainty in their membership due to overlapping fields. Fifteen clusters were either poorly defined or invisible on the plate and were rejected. The remaining 88 clusters are listed in Table I. Column 1 contains the cluster name, columns 2 and 3 the 1950 coordinates, column 4 the galactic latitude, column 5 the cluster redshift, and column 6 the associated radio source, if any.

TABLE I

THE CLUSTERS STUDIED

(1) Cluster	(2) α	(3) β	(4) b	(5) z	(6) Radio
Zw499-13	0016	+2947	-32.3	.0226	
Zw478-5	0019	+2207	-40.0	.0207	
Zw457-27	0024	+1654	-45.3	.29	
Zw457-28	0024	+1654	-45.3	.392	
A31	0025	+2223	-39.9	.1592	3C381
A76	0036	+0612	-56.3	.0377	
A115	0053	+2604	-36.5	.1959	3C28
A119	0054	-0130	-64.1	.0446	3C29
A147	0106	+0126	-60.9	.0441	
0106+13	0106	+1304	-49.3	.0600	3C33
A151	0106	-1536	-77.6	.0526	
0117+31	0117	+3155	-30.3	.0591	4C31.04
A195	0126	+1842	-43.0	.0437	PKS0124+18
A234	0138	+1840	-42.4	.1731	
A272	0152	+3340	-27.1	.0877	
A278	0154	+3201	-28.6	.0904	
A376	0242	+3627	-20.8	.0487	
A400	0255	+0552	-44.9	.0231	
A407	0258	+3540	-20.0	.0473	
A465	0348	+0613	-35.2	.0855	
A505	0452	+7959	22.2	.0543	
A539	0513	+0555	-18.2	.0267	
A548	0546	-2534	-24.6	.0391	
A553	0608	+4841	14.0	.0670	
A568	0705	+3506	18.4	.0779	
A576	0718	+5518	26.2	.0404	
A592	0740	+0930	15.6	.0621	
Zw118-3	0801	+2523	26.4	.0599	3C192
A634	0812	+5818	33.8	.0266	
A646	0818	+4716	34.5	.1303	3C197.1
Zw32-7	0820	+0647	23.3	.0809	3C198
A671	0825	+3037	33.0	.0497	
A665	0826	+6606	34.6	.1832	
A732	0855	+0321	29.3	.2030	
A754	0906	-0926	24.7	.0537	

Table I (continued) The Clusters Studied

(1) Cluster	(2) α	(3) β	(4) b	(5) z	(6) Radio
Zw238-18	0918	+4548	44.8	.1745	3C218
A838	0935	-0449	33.2	.0507	
Zw211-58	1010	+3922	55.0	.0222	
A993	1019	-0440	41.6	.0530	
A1020	1024	+1039	52.1	.0650	
A1132	1055	+5702	54.2	.1363	
A1139	1055	+0147	52.6	.0376	
A1185	1107	+2852	67.5	.0349	
A1228	1118	+3422	69.3	.0344	
A1257	1124	+3538	70.2	.0339	
A1314	1132	+4921	63.5	.0335	
A1377	1145	+5559	59.2	.0509	
A1413	1153	+2341	76.8	.1427	
Zw41-22	1215	+0400	65.2	.0766	MSH12+04
A1553	1228	+1050	72.7	.1652	
A1589	1239	+1852	81.2	.0718	
A1643	1253	+4422	73.0	.1981	
A1656	1257	+2814	88.0	.0230	
Zw160-23	1300	+3213	84.6	.0950	
A1677	1304	+3110	85.0	.1832	
Zw160-43	1306	+2716	86.2	.2394	3C284
A1689	1309	-0105	61.1	.1747	
1319+42	1319	+4251	73.4	.0797	3C285
A1736	1324	-2653	35.1	.0431	
A1775	1341	+2626	78.4	.0718	
1359-11	1359	-1128	47.6	.025	PKS1358-11
1410+52	1410	+5224	60.8	.4619	3C295
A1904	1420	+4837	62.4	.0719	
A1930	1431	+3146	67.5	.1313	
Zw134-20	1448	+2617	63.5	.369	
A1983	1450	+1657	60.2	.0458	3C306
A2048	1513	+0433	48.8	.0945	
A2052	1514	+0712	50.2	.0351	3C317
A2065	1520	+2754	56.7	.0722	
A2100	1534	+3749	54.0	.1533	

Table I (continued) The Clusters Studied

(1) Cluster	(2) α	(3) β	(4) b	(5) z	(6) Radio
Zw136-2	1545	+2104	49.6	.267	3C323.1
A2151	1603	+1755	44.5	.0360	
A2162	1610	+3000	46.2	.0318	
A2165	1612	+2636	45.1	.1286	
A2199	1627	+3939	43.7	.0312	
A2197	1628	+4055	43.5	.0303	
A2266	1723	+3208	31.4	.1671	3C357
2059-28	2059	-2813	-39.6	.0379	PKS2058-28
Zw430-21	2247	+1107	-41.4	.0255	PKS2247+11
Zw430-20	2250	+1116	-41.8	.3271	PKS2251+11
Zw430-10	2256	+1350	-40.5	.0331	3C455
Zw406-13	2308	+0720	-47.5	.0428	
A2593	2322	+1425	-43.2	.0440	
A2597	2323	-1224	-64.9	.0825	MSH23-112
A2634	2336	+2646	-33.1	.0307	3C465
A2657	2343	+0852	-50.4	.0414	
A2666	2348	+2652	-33.8	.0273	
A2670	2352	-1036	-68.5	.0753	

In addition to the 48 inch sample, seven clusters photographed on the Palomar 200 inch telescope with the 90 mm image tube at the prime focus, were kindly made available to me by Professors Gunn and Oke.

Data reduction proceeded as follows. The plates were inspected and the clusters identified. Using the cluster redshift, H = 55 km/sec/Mpc, and $q_o = 0$, a 3 Mpc circle was drawn on the back of each plate, centered on the cluster. Within this circle, x-y positions were measured with a grid, to an accuracy of about .2 mm, for the fourty brightest (as estimated visually) galaxies not brighter than the brightest cluster galaxy. To estimate the number of field galaxies in the sample, circles of the same radius, space permitting, were drawn surrounding the cluster. In each of these circles, the number of galaxies within the magnitude range of the 40 galaxies in the cluster sample were counted. The mean number for all surrounding circles was taken to be N_f, the number of field galaxies in the sample. Occasionally smaller circles had to be used. The counts were then multiplied by the ratio of the areas. From the measured positions, all possible separations were computed and the values of λ determined.

IV. DATA ANALYSIS

The models we chose to test are zero pressure Friedmann models with zero cosmological constant. The cosmology is then specified by the present Hubble constant $H_o = (\dot{R}/R)_o$ and deceleration parameter $q_o = -(\ddot{R}R/\dot{R}^2)_o$ where R is the scale factor in the metric

$$ds^2 = c^2\,dt^2 - R^2(t)\left[du^2 + \sigma^2(u)(d\theta^2 + \sin^2\theta\, d\phi^2)\right]. \qquad (8)$$

We adopt the value $H_o = 55$ km/sec/Mpc in our analysis. It makes no difference to the value of q_o, however, as all dependence on the Hubble constant is absorbed in the mean metric cluster size λ_o, determined from the data.

To determine what value of q_o is most consistent with our observations, we compare the predictions of a series of trial models, with varying q_o, to the observed cluster sizes. The model with the minimum residuals then fixes q_o. Our procedure is as follows. The angular size θ of an object at a cosmological redshift z is related to its metric size ℓ by

$$\theta = \ell\,\frac{H_o}{c}\,(1+z)^2 q_o^2\left\{q_o z + (q_o - 1)\left[\sqrt{(1+2q_o z)} - 1\right]\right\}^{-1} \qquad (9)$$

for $q_o > 0$ and

$$\theta = \ell\,\frac{H_o}{c}\,\frac{(1+z)^2}{z(1+z/2)} \qquad \text{for } q_o = 0. \qquad (10)$$

In measuring our clusters we chose an angular cutoff radius corresponding to ℓ = 3 Mpc in equation (9). For $q_o \neq 0$, however, this angular size corresponds to a metric radius of

$$R_c\,(\mathrm{Mpc}) = \frac{3}{z(1+z/2)}\,\frac{1}{q_o^2}\left\{q_o z + (q_o-1)\left[\sqrt{(1+2q_o z)}-1\right]\right\}. \quad (11)$$

This value of R_c is used in equation (7) to determine r_o for each cluster. The "corrected" size λ_r is then computed from equation (7) using R_c = 3, and N_f = 0. From our definition of λ,

$$\lambda = \frac{cz}{H_o}\,\frac{1+z/2}{(1+z)^2}\,\theta \quad (12)$$

where θ is the angular size of the cluster, so the values of λ_r must be compared to the values of the function

$$F(q_o,z) = z\left(1+\frac{z}{2}\right)q_o^2\left\{q_o z + (q_o-1)\left[\sqrt{(1+2q_o z)}-1\right]\right\}^{-1} \quad (13)$$

The cluster sizes λ_{ri} are distributed about a mean value λ_o. These are determined by minimizing the residuals

$$\chi^2 = \sum_{i=1}^{N_{cl}} \frac{1}{\sigma_i^2}\left(\log \lambda_{r_i} - \log F_i - \log \lambda_o\right)^2 \quad (14)$$

where $N_{c\ell}$ is the number of clusters, 95. The variance σ_i^2 for each cluster is taken as the mean value from the data weighted by the background correction factor from §II b:

$$\sigma_i^2 = \frac{\sigma^2 (1+\varepsilon_i)^2 N_{cl}}{\sum_{i=1}^{N_{cl}} (1+\varepsilon_i)^2} . \tag{15}$$

For each trial model, λ_o may be determined directly from the relation

$$\log \lambda_o = \frac{\sum_i \frac{1}{\sigma_i^2} (\log \lambda_{ri} - \log F_i)}{\sum_i \frac{1}{\sigma_i^2}} . \tag{16}$$

q_o is then determined by comparing the residuals from various models. The standard deviation of q_o and λ_o is determined by considering χ^2 and $\log \lambda_o$ as functions of q_o. Details are given in Appendix A.

V. RESULTS FOR NO EVOLUTION

The χ^2 residuals are plotted against q_o in Figure 3. Negative values of q_o are obtained by extending equation (13) by analytic continuation, and do not represent physical models. The residuals for the steady state model ($F(z) = (1 + z/2)/(1+z)$) are indicated by the circle at

FIGURE 3

Least-squares analysis. χ^2 residuals are plotted against test values of q_o. The circle denotes the steady state model.

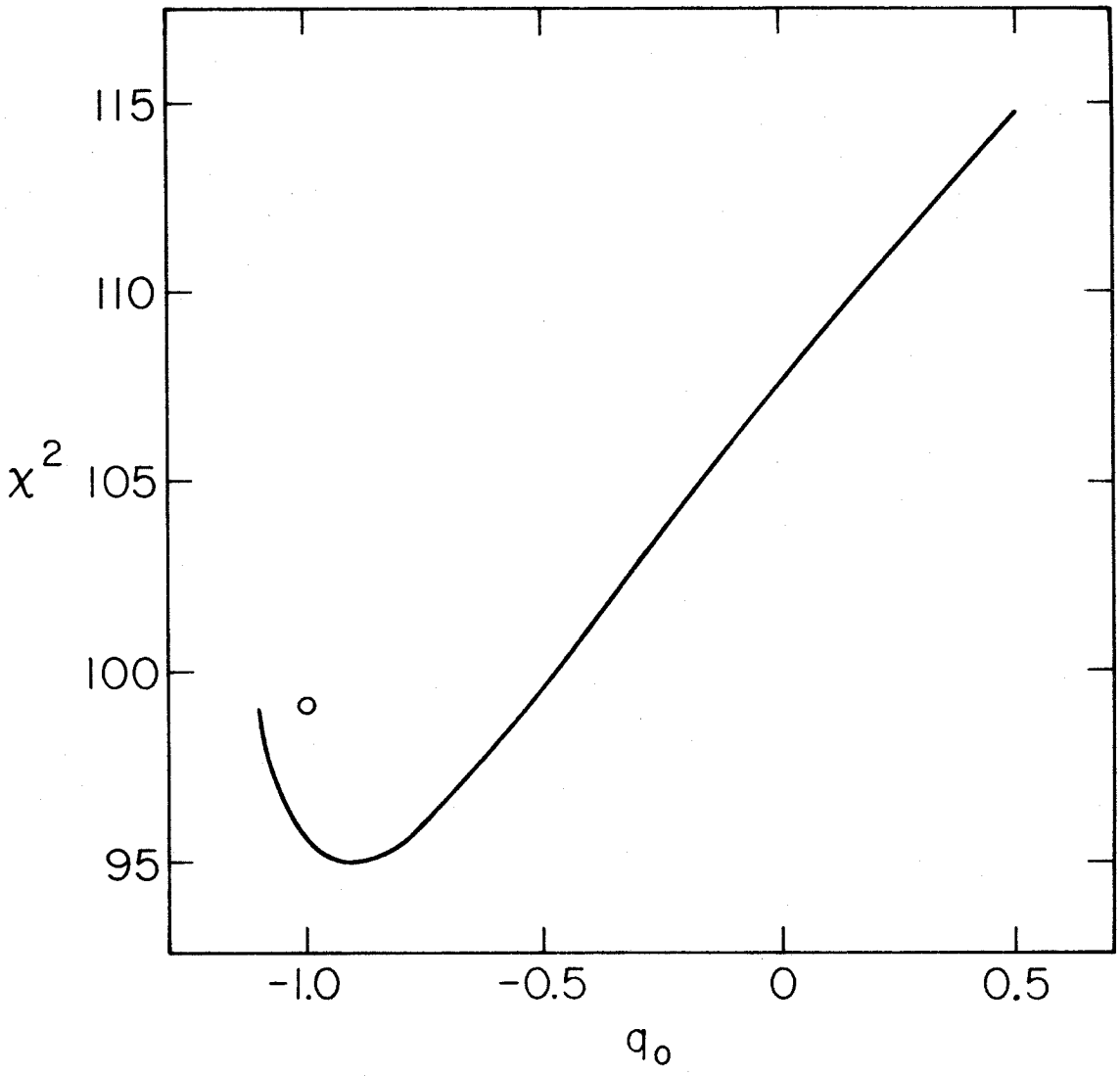
115
110
105
100
95
χ^2
o
-1.0
-0.5
0
0.5
q_o

$q_o = -1$. Over the range of redshifts considered here, the steady state is very similar to the $q_o = -.5$ Friedmann model. In Figure 4 we plot the corrected sizes λ_r for four models with $q_o = .5$, 0, -.5 and -1 (not the steady state). The solid line in each case is the function log F + log λ_o for the appropriate model, λ_o in each case having been determined from equation (16). The best least squares fit to the data is

$$q_o = -.90 \pm .18$$
$$\log \lambda_o = -.015 \pm .010 \qquad (17)$$

The sensitivity of the function $F(q_o)$ to q_o increases rapidly as q_o approaches -1 (as described in Appendix A). If the best least squares fit had resulted in $q_o = 0$, the standard deviation of q_o would have been $\sigma_{q_o} = .4$. The results for our clusters are presented in Table II. Column 1 contains the cluster name, column 2 the redshift, column 3 the estimated number of contaminating field galaxies N_f, column 4 the measured size log λ, and column 5 the corrected size log λ_r for $q_o = -.9$.

The above results are for no evolution, and are presented here because of the present uncertainty of evolutionary corrections. Let us now consider the possible effects of evolution in the cluster sizes on this result.

FIGURE 4

The angular size redshift diagram. The reduced cluster size is plotted against redshift for four values of the deceleration parameter. Open circles represent the 200-inch clusters of Gunn and Oke.

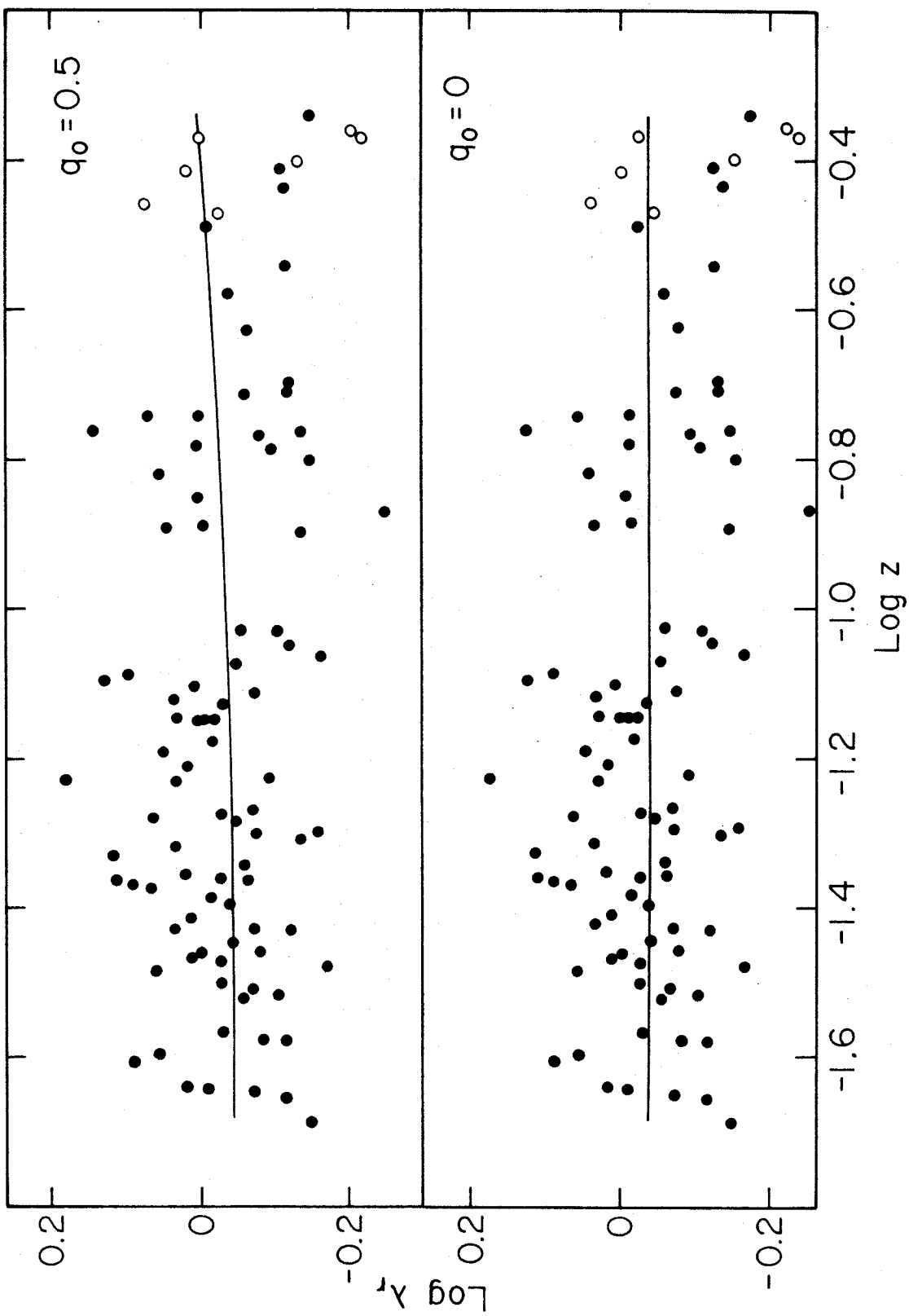
$q_o = 0.5$
$q_o = 0$
Log λ_r
Log z
0.2
0
-0.2
-1.6
-1.4
-1.2
-1.0
-0.8
-0.6
-0.4

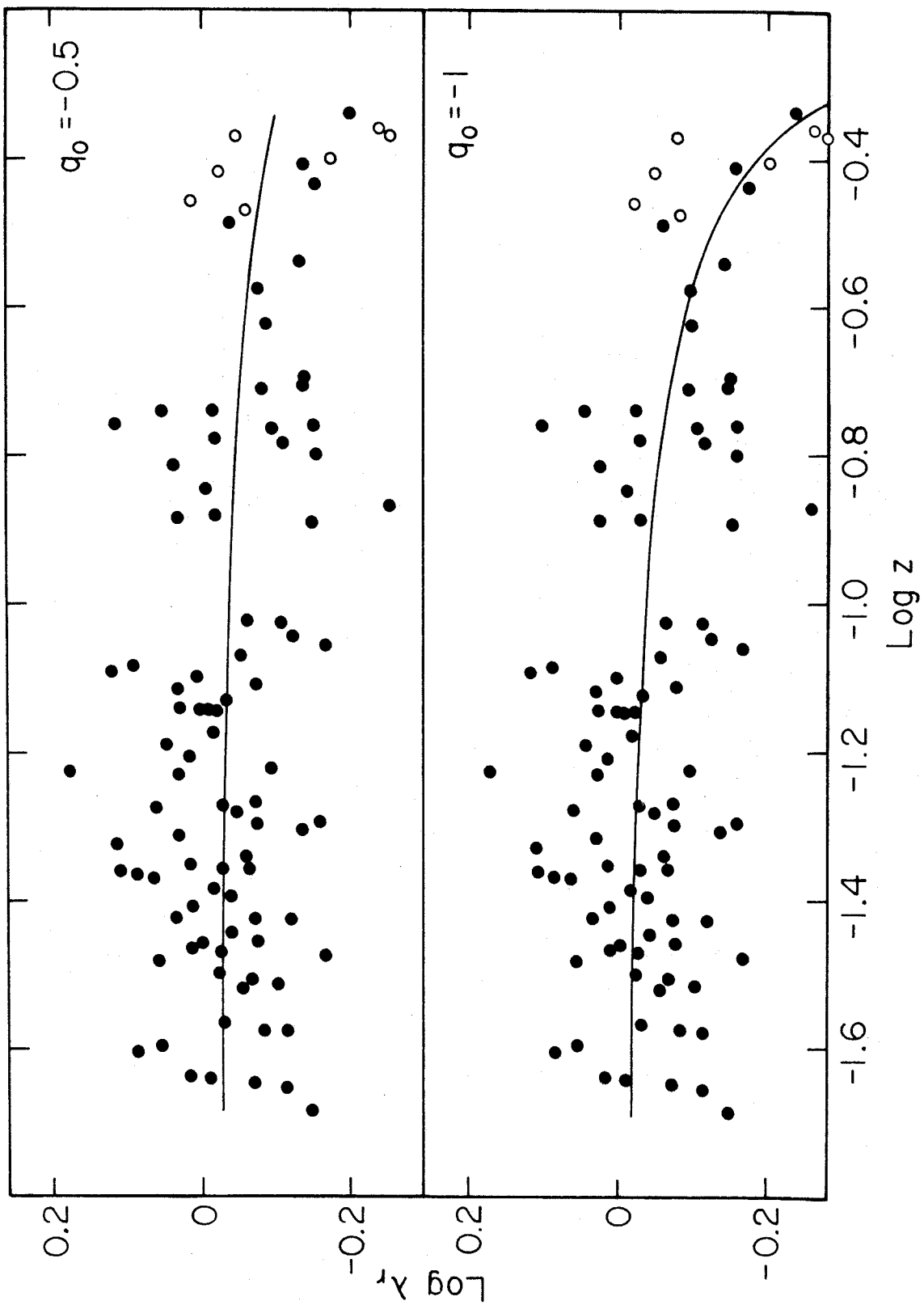
q_o=-0.5
q_o=-1
Log λ_r
Log z
0.2
0
-0.2
-1.6
-1.4
-1.2
-1.0
-0.8
-0.6
-0.4

TABLE II

THE CLUSTER SIZES

(1) Cluster	(2) z	(3) N_f	(4) $\log\lambda$	(5) $\log\lambda_r$
Zw478-5	.0207	3	-.108	-.148
Zw211-58	.0222	4	-.108	-.115
Zw499-13	.0226	5	-.016	-.071
A1656	.0230	3	.019	-.010
A400	.0231	4	.051	.016
1359-11	.0250	7	.127	.086
Zw430-21	.0255	3	.077	.054
A634	.0266	4	-.066	-.116
A539	.0267	5	-.027	-.084
A2666	.0273	10	.061	-.032
A2197	.0303	7	.016	-.056
A2634	.0307	6	-.033	-.103
A2199	.0312	7	.006	-.069
A2162	.0318	5	.024	-.025
Zw430-10	.0331	5	.093	.057
A1314	.0335	4	-.113	-.167
A1257	.0339	4	.014	-.026
A1228	.0344	5	.055	.011
A1185	.0349	6	.052	.002
A2052	.0351	5	-.021	-.078
A2151	.0360	4	.001	-.041
A1139	.0376	5	-.058	-.120
A76	.0377	7	.003	-.073
2059-28	.0379	4	.067	.034
A548	.0391	3	.039	.012
A576	.0404	6	.022	-.038
A2657	.0414	5	.032	-.016
Zw406-13	.0428	6	.105	.064
A1736	.0431	6	.124	.088
A195	.0431	6	.140	.108
A2593	.0440	5	.022	-.028
A147	.0441	7	.010	-.064
A119	.0446	9	.088	.015
A1983	.0458	6	.004	-.060
A407	.0473	7	.148	.112

Table II (continued) The Cluster Sizes

(1) Cluster	(2) z	(3) N_f	(4) $\log\lambda$	(5) $\log\lambda_r$
A376	.0487	5	.072	.031
A671	.0497	6	-.060	-.135
A838	.0507	5	.018	.074
A1377	.0509	5	-.092	-.158
A151	.0526	4	-.004	-.047
A993	.0530	5	.097	.061
A754	.0537	4	.013	-.028
A505	.0543	7	.004	-.072
0117+31	.0591	6	.078	.029
Zw118-3	.0597	6	.191	.174
0106+13	.0600	6	-.024	-.094
A592	.0621	5	.060	.016
A1020	.0650	6	.091	.045
A553	.0670	5	.032	-.017
A1589	.0718	3	.011	-.020
A1775	.0718	6	.055	.000
A1904	.0719	7	.054	-.011
A2065	.0722	5	.071	.029
A2670	.0753	4	.009	-.033
Zw41-22	.0766	5	.073	.031
A568	.0779	7	.002	-.076
1319+42	.0797	9	.081	.002
Zw32-7	.0809	7	.155	.119
A2597	.0825	7	.132	.088
A465	.0855	10	.047	-.055
A272	.0877	8	-.062	-.166
A278	.0904	8	-.026	-.123
A2048	.0945	9	-.005	-.111
Zw160-23	.0950	8	.024	-.062
A2165	.1286	12	-.002	-.152
A646	.1303	9	.103	.028
A1930	.1313	10	.073	-.024
A1132	.1363	8	-.137	-.256
A1413	.1427	6	.051	-.009
A2100	.1533	10	.114	.030

Table II (continued) The Cluster Sizes

(1) Cluster	(2) z	(3) N_f	(4) $\log\lambda$	(5) $\log\lambda_r$
A31	.1596	6	-.075	-.157
A1553	.1652	10	.007	-.114
A2266	.1671	12	.093	-.025
A234	.1731	11	.027	-.103
Zw238-18	.1745	12	-.003	-.157
A1689	.1747	10	.169	.106
A665	.1832	7	.107	.048
A1677	.1832	8	.061	-.021
A115	.1959	11	.039	-.089
A1643	.1981	12	.009	-.144
A732	.2030	11	-.003	-.144
Zw160-43	.2394	10	.028	-.094
Zw136-2	.267	14	.078	-.091
Zw457-27	.29	8	-.029	-.139
Zw430-20	.3271	10	.067	-.054
Zw134-20	.369	12	.004	-.169
Zw457-28	.392	9	-.019	-.151
1410+52	.4619	14	-.001	-.224

VI. EVOLUTIONARY EFFECTS

It is generally accepted that at any given distance we see clusters in varying evolutionary phases. This is probably a consequence of the dispersion in cluster collapse times resulting from the spectrum of densities of the pre-cluster perturbations at recombination (Gunn and Gott, 1972) As discussed in Part I the varying cluster types and characteristics are probably largely a result of varying evolutionary phases. This allows us to estimate the maximum possible effect of evolution on the cluster sizes. If we accept that all evolutionary phases of a cluster are present in our nearby sample ($z < .1$) then it follows that in this sample we should see clusters in their oldest evolutionary phases (the clusters that were the first to collapse and thus have evolved for the greatest number of collapse times) and also clusters in very early evolutionary phases (those pre-collapse clusters that have just reached sufficient density to be recognizable as clusters). As we look back in time with increasing distance, distant clusters must fall within these evolutionary extremes. If there were a significant evolutionary correction to the cluster sizes, we would expect the more distant clusters to show less dispersion than the nearby clusters as they do not contain clusters as old as some of the nearby ones. This trend

is in fact observed. After correcting for background galaxies (which make the dispersion larger than it should be) we find a difference of $\Delta\sigma_{\ln\lambda_r} \simeq .05$ between the dispersion of the 14 most distant clusters, and the dispersion of the nearest clusters. This could be attributed to evolutionary effects, and results in a change in q_o of about .1.

The same argument holds for selection effects. Given the assumption that all cluster types are represented in the nearby sample, it follows that any selection effects in the more distant clusters will reduce the dispersion of their sizes. The data then limit the combined effect of possible evolutionary or selection effects to $\Delta\sigma_{\ln\lambda_r} \simeq .05$ or $\Delta q_o \simeq .1$ (at $q_o = -.9$).

Let us now consider possible evolutionary effects. For convenience we adopt the term "positive" for those that would increase q_o and "negative" for those effects that would decrease it. Evolution in the cluster sizes can result from two effects: 1) The size λ_r of a cluster will be a function of the "relative age" of a cluster $\tau \equiv t/t_c$ where t_c is the cluster collapse time, and 2) The size of a cluster may depend on its collapse time t_c (i.e., by initial conditions at recombination).

To investigate the first effect we have calculated the size λ_r of a numerically simulated collapsing cluster due to

Aarseth. One hundred points distributed randomly within a sphere were released and followed through collapse. The size is calculated at various times from the projected positions of the 40 most massive points within a 3 Mpc circle. The results are shown in Figure 5. After going through a minimum at the collapsed phase, the size returns to about half of the pre-collapse maximum then decreases at a rate of about 4% per collapse time. The slow decrease in size after collapse is primarily due to two body relaxation which removes energy from the core.

The effect of initial conditions on cluster sizes can be approached theoretically. In the standard picture of cluster formation (Gunn and Gott, 1972) the size scale of a cluster for any fixed relative age τ is proportional to

$$R \sim t_c^{\frac{2}{3}} \tag{18}$$

where

$$t_c \sim \rho_+^{-\frac{3}{2}} \tag{19}$$

and ρ_+ is the density perturbation above the critical density $3H^2/8\pi G$. If , following Peebles (1974), Press and Schecter (1974), and Gott (1975), we assume a white noise spectrum of density perturbations, we obtain for the distribution of collapse times

$$P(t_c) \sim t_c^{-\frac{5}{3}} \tag{20}$$

FIGURE 5

Numerical simulation of cluster evolution. The reduced cluster size is shown as a function of the relative age of the cluster.

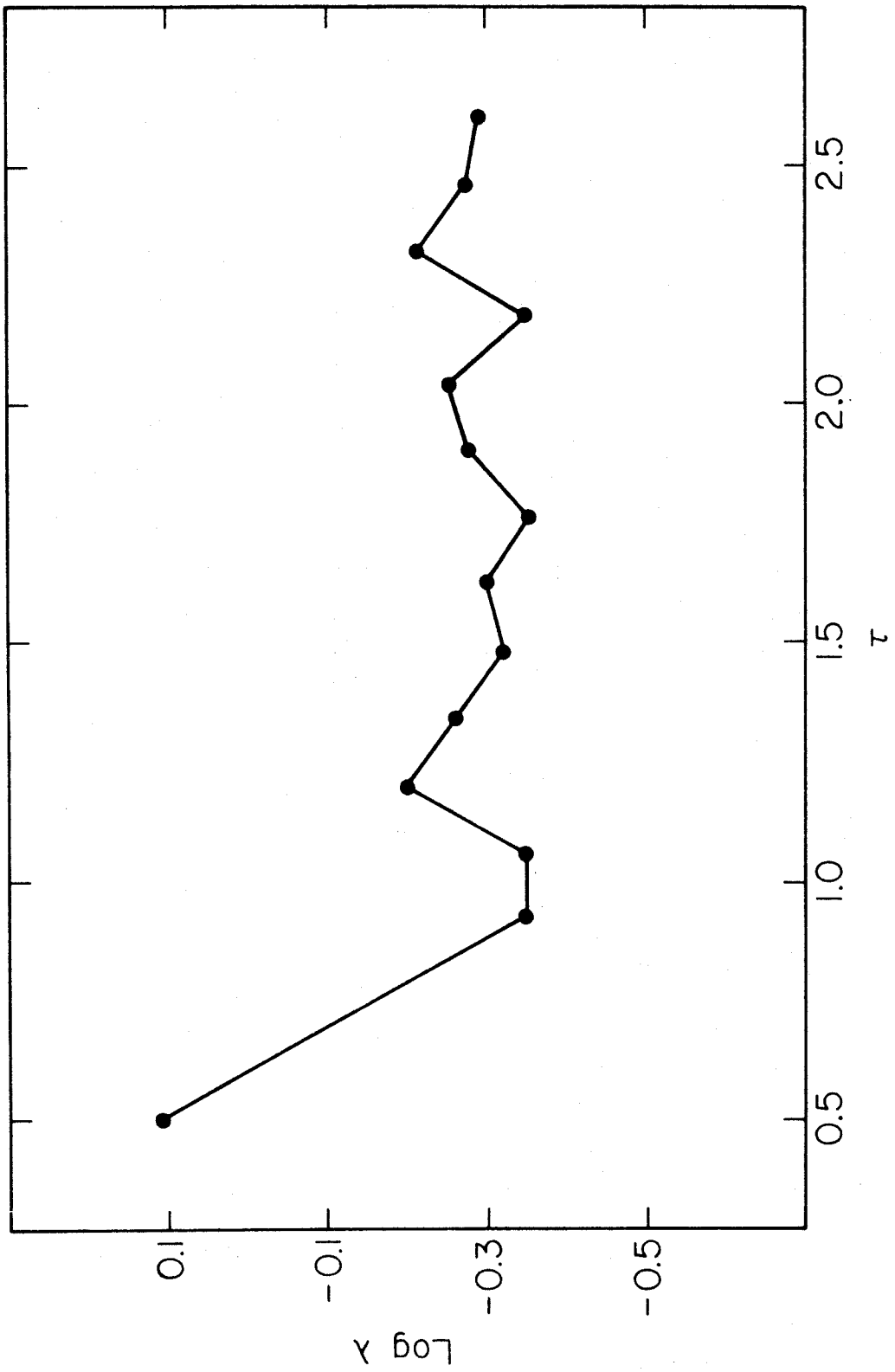
0.1
-0.1
-0.3
-0.5
Log λ
0.5
1.0
1.5
2.0
2.5
τ

The distribution of relative ages at any time t then is

$$P(\tau) \sim \tau^{-\frac{1}{3}}. \tag{21}$$

Thus we have the evolutionary picture shown in Figure 6. As time progresses, new clusters enter our sample when they reach sufficient density to be recognizable. These clusters however are larger as they have longer collapse times (equation (18)). The size of any given cluster may be written

$$\lambda \sim t_c^{\frac{2}{3}} f(\tau) \tag{22}$$

where $f(\tau)$ is the function illustrated in Figure 5. At any fixed time t, the mean value of $\ln\lambda_r$ will be

$$\langle \ln \lambda_r \rangle = \frac{\int_\alpha^\beta \ln \lambda_r \, P(\tau)\, d\tau}{\int_\alpha^\beta P(\tau)\, d\tau} = \frac{2}{3}\ln t + \frac{\int_\alpha^\beta \ln(\tau^{-\frac{2}{3}} f(\tau)) P(\tau)\, d\tau}{\int_\alpha^\beta P(\tau)\, d\tau} \tag{23}$$

where α is the relative age at which a cluster enters our sample (assumed constant), and $\beta(t) = t/t_{cmax}$ is the relative age of the oldest cluster in our sample. The

FIGURE 6

Cluster evolution. Sizes of clusters in our sample are shown as a function of cosmic time.

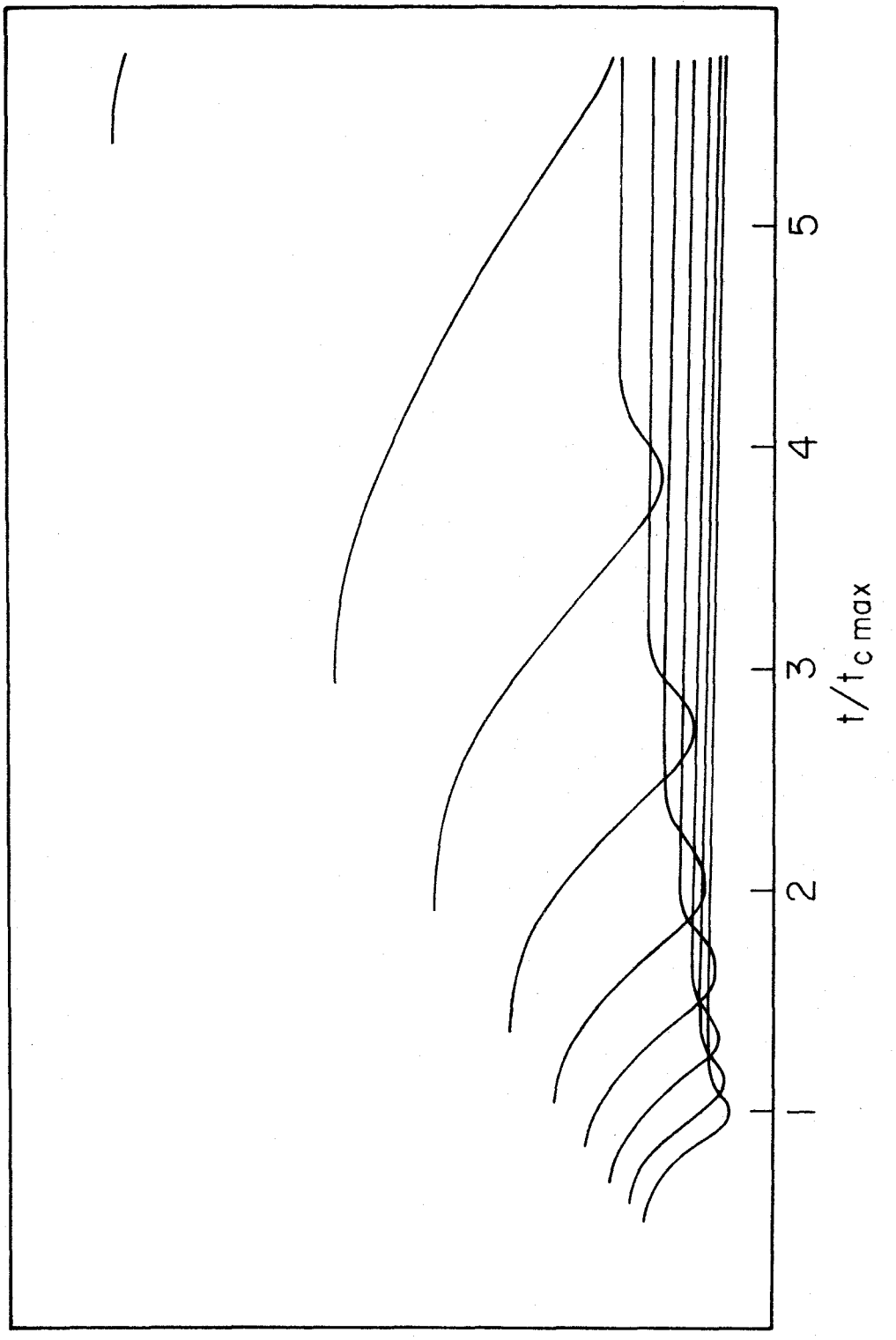
1
2
3
4
5
$t/t_{c\,max}$
λ

only t dependence in the integrals in equation (23) is through the upper limit, i.e., the oldest clusters. For large τ,

$$f(\tau) \sim e^{-\frac{\tau}{\tau_o}} \tag{24}$$

where τ_o is the decay time from two body relaxation. A least squares fit to the 11 post-collapse data points of Figure 5 gives

$$\tau_o \simeq 30. \tag{25}$$

Evaluating equation (23) we obtain to first order in α/β

$$\langle \ln \lambda_r \rangle = -\frac{2}{5}\frac{\beta}{\tau_o}\left[1+\left(\frac{\alpha}{\beta}\right)^{\frac{2}{3}}\right] - \frac{2}{3}\ln\left(\frac{\beta}{\alpha}\right)\left(\frac{\alpha}{\beta}\right)^{\frac{2}{3}} + \text{const},$$

$$\text{hence } \frac{\Delta\langle \ln \lambda_r \rangle}{\Delta \beta} \simeq -\frac{2}{5\tau_o}\left[1+\frac{1}{3}\left(\frac{\alpha}{\beta}\right)^{\frac{2}{3}}\right] + \frac{2}{3\beta}\left[\frac{2}{3}\ln\left(\frac{\beta}{\alpha}\right)-1\right]\left(\frac{\alpha}{\beta}\right)^{\frac{2}{3}}. \tag{26}$$

The first term in equation (26) represents negative evolution due to the shrinking of the cores of the collapsed clusters by two body relaxation. The second term represents positive evolution due to young clusters with longer collapse times entering our sample. Both effects are small, and tend to cancel. Our oldest clusters have probably evolved for the order of 10 collapse times, or 10^{10} years

so $\beta \simeq 10$ and $t_{cmax} = 10^9$. With these values we obtain

$$\frac{\Delta\langle \ln \lambda_r \rangle}{\Delta t} \simeq \frac{-.014 + .018}{t_{c\,max}} = \frac{.004}{t_{c\,max}} . \tag{27}$$

Over the range of our data this becomes

$$\Delta_{ev} \langle \ln \lambda_r \rangle \simeq .04 \tag{28}$$

which is surprisingly close to our estimate obtained from the dispersions. Including this evolutionary correction would raise q_o to

$$q_o = -.8 \tag{29}$$

An effect that may not be properly represented by the numerical models is that of dynamical friction (Ostriker and Tremain, 1976, White, 1976). The effect of galaxy coalescence on the parameter λ_r is uncertain, but may result in positive evolution. Also, tidal stripping in the center of dense clusters (Richstone, 1975) may reduce the magnitude of central galaxies. Some of these may then drop out of our sample of the forty brightest galaxies causing λ_r to increase. Mass loss from this effect would, however, occur primarily in the outermost regions of the galaxies, and thus would have a less pronounced effect on our visually estimated magnitudes. The timescales associated with these processes are rather uncertain, and more work is needed in this area.

VII. DISCUSSION

Let us summarize our results. We have outlined a cosmological test that can make use of a large number of clusters of galaxies to determine q_o to a relatively high degree of accuracy. The test suffers from relatively few systematic uncertainties, the primary ones being evolution and selection effects. From our cluster sample we obtain a pre-evolution value for q_o of -.9 with a standard deviation of .2 (.4 at $q_o = 0$). Our best estimate of evolution in the cluster sizes increases q_o to -.8. The steady state model is consistent with the data, but does not produce the best least squares fit.

The dispersions in the cluster sizes suggest that no major evolutionary effects or selection effects in cluster types are present in the data. This does not preclude selection effects in cluster richness, as not all richness classes are present in the nearby sample. An analysis of the residuals in the sizes of Abell clusters in our sample, however, shows no systematic dependence of the cluster sizes on richness class. The existance of a size-richness effect of sufficient magnitude to raise q_o to 0 appears very unlikely, but further observations are needed to determine definitive limits for such an effect.

All that remains that may affect our result is possible

subjective bias in selecting the galaxies that represent each cluster, or in estimating the background. In principle none should exist as the method is completely objective. The galaxy magnitudes, however, have been estimated visually so some margin for error exists, but we believe it to be small. Removing the seven 200 inch clusters from the sample gives $q_o = -.94$, and even removing the three smallest, most distant cluster does not raise q_o above -.5. Clearly, the inclusion of more distant clusters in our sample would increase the power of the test, and the weight of its results.

A possible way of extending this test to greater distances would be by applying it to distant clusters with associated quasars. Clusters too distant to have redshifts measured can still be measured by our technique to determine their sizes. The sizes can then be plotted against quasar redshift in the angular size-redshift test. If the quasar redshift is cosmological, it should be representative of the cluster (Oemler, Gunn and Oke, 1972, Gunn, 1971), and would provide a strong cosmological test. Conversely, agreement with other determinations of q_o would support the cosmological hypothesis for quasar redshifts.

APPENDIX A

Statistical Reductions

The best value of q_o and λ_o are those which minimize the quantity

$$\chi^2 = \sum_{i=1}^{N_{cl}} \frac{1}{\sigma_i^2} \left(\log \lambda_{ri} - \log F_i - \log \lambda_o \right)^2 . \qquad (1)$$

The condition $\dfrac{\partial \chi^2}{\partial \log \lambda_o} = 0$ leads to

$$\log \lambda_o = \frac{\sum_{i=1}^{N_{cl}} \frac{1}{\sigma_i^2} \left(\log \lambda_{ri} - \log F_i \right)}{\sum_{i=1}^{N_{cl}} \frac{1}{\sigma_i^2}} . \qquad (2)$$

The errors σ_i, for each cluster, are determined from

$$\sigma_i^2 = \sigma^2 \frac{(1+\varepsilon_i)^2 N_{cl}}{\sum_{i=1}^{N_{cl}} (1+\varepsilon_i)^2} \quad , \quad \sigma^2 = \sum_{i=1}^{N_{cl}} \sigma_i^2 \quad . \qquad (3)$$

For each trial run, $\log \lambda_o$ is determined, and $\chi^2(q_o)$ evaluated.

The errors in q_o and $\log \lambda_o$ are determined by the relations

$$\sigma_x^2 = \sigma^2 \left(D^{-1}\right)_{xx} \tag{4}$$

where
$$D_{xy} = \sum_i \left(\frac{\partial g_i}{\partial x}\right)\left(\frac{\partial g_i}{\partial y}\right) \quad ,$$
$$g_i = \frac{\sigma}{\sigma_i}\left(\log \lambda_{ri} - \log F_i - \log \lambda_o\right) \quad . \tag{5}$$

This gives
$$D_{qq} = \frac{\sigma^2}{2}\frac{\partial^2}{\partial q_o^2}\left(\chi^2\right) \quad , \quad b \equiv \log \lambda_o \quad ,$$
$$D_{bb} = \sum_i \frac{\sigma^2}{\sigma_i^2} = \frac{1}{N_{cl}} \sum_i (1+\varepsilon)^2 (1+\varepsilon)^{-2} \quad , \tag{6}$$
$$D_{bq} = D_{qb} = D_{bb}\frac{\partial b}{\partial q_o}$$

which are easily evaluated from the trial runs. When evaluated at our "best fit" value of $q_o = -.90$, the formal error in q_o is $\sigma_{q_o} = .18$. This should not be directly compared with previous determinations that place q_o near zero, because of the increased sensitivity of the function $F(q_o)$ for negative values of q_o. The errors at different values of q_o may be computed by means of the relation

$$\frac{\partial \ln \lambda}{\partial q_o} = \frac{2}{q_o} - \frac{z + \sqrt{(1+2q_oz)} - 1 + (q_o-1)(1+2q_oz)^{-\frac{1}{2}} z}{q_o z + (q_o-1)\left[\sqrt{(1+2q_oz)} - 1\right]} \tag{7}$$

Values of this quantity are listed in Table AI for a range of q_o and z. Applying equation (9) to our distant clusters gives $\sigma_{q_o} = .4$ at $q_o = 0$.

TABLE AI

$$\frac{\partial \ln \lambda}{\partial q_o}$$

q_o	z = .2	z = .3	z = .4	z = .5	z = .6
.5	.095	.138	.179	.217	.253
.4	.097	.143	.187	.230	.270
.3	.100	.149	.197	.244	.289
.2	.103	.155	.208	.260	.311
.1	.106	.162	.220	.278	.338
.0	.109	.170	.233	.300	.369
-.1	.113	.178	.249	.326	.408
-.2	.116	.187	.267	.357	.457
-.3	.120	.198	.288	.395	.521
-.4	.125	.209	.314	.444	.608
-.5	.129	.223	.345	.508	.737
-.6	.134	.238	.383	.435	.950
-.7	.140	.256	.433	.734	1.393
-.8	.146	.278	.500	.971	3.333
-.9	.153	.304	.597	1.532	
-1.0	.160	.336	.752		

REFERENCES

Austin, T. B., and Peach, J. V. 1974, M.N.R.A.S., 167, 437.

Bahcall, N. 1975, Ap.J., 198, 249.

de Vaucouleurs, G. 1948, C.R. Acad. Sci. Paris, 227, 586.

Gott, J. R. 1975, Ap.J., 201, 296.

Gunn, J. E. 1971, Ap.J. (Letters), 164, L113.

Gunn, J. E., and Gott, J. R. 1972, Ap.J., 176, 1.

Gunn, J. E., Oke, J. B. 1975, Ap.J., 195, 255.

King, I. R. 1972, Ap.J. (Letters), 174, L123.

Noonan, T. W. 1972, A.J., 77, 134.

Oemler, A., Gunn, J. E., and Oke, J. B. 1972, Ap.J. (Letters), 176, L47.

Ostriker, J. P., and Tremaine, S. D. 1976, Ap.J. (Letters), 202, L13.

Peach, J. V., and Beard, J. M. 1969, Ap. Letters, 4, 205.

Peebles, P. J. E. 1974, Ap.J. (Letters), 189, L51.

Press, W. H., and Schechter, P. 1974, Ap.J., 187, 425.

Richstone, D. O. 1975, Princeton Ph.D. Thesis

Sandage, A. 1961, Ap.J., 133, 355.

Sandage, A., and Hardy, E. 1973, Ap.J., 183, 743.

White, D. M. 1976, (Preprint).

Zwicky, F. 1957, Morphological Astronomy (Berlin: Springer Verlag).

Zwicky, F., Herzog, E., Wild, P., Karpowicz, M., and Kowal, C. T. 1961-1968, Catalogue of Galaxies and Clusters of Galaxies, in 6 volumes. (Pasadena: California Institute of Technology.)